UNIVERSITY OF OTTAWA

Effects of Weathering on Leaching Properties of Slag from a Niobium Mine, Oka, Quebec.

By

Hannah Balkwill Tweedie

A THESIS SUBMITTED TO THE UNIVERSITY OF OTTAWA IN PARTIAL FULFILLMENT OF THE REQUIREMENTS FOR THE DEGREE OF MASTER OF SCIENCE

DEPARTMENT OF EARTH AND ENVIRONMENTAL SCIENCES OTTAWA, ONTARIO
Jan 2020

Abstract

Between 1961 and 1976 niobium ore was mined by the St. Lawrence Columbium Group in the community of Oka, located approximately 50 km W of Montreal, Quebec. Ferroniobium was formed through aluminothermic reduction of pyrochlore-group minerals. This process produced circular slag casts that were discarded in a small dump at the mine site. This work is designed to provide knowledge with respect to the long-term stability of Oka slag and the reaction processes that control drainage water chemistry in slag disposal areas. The slag casts were sampled at the top, middle, and bottom based on the expectation that fractional crystallization had influenced the mineralogy and geochemistry during the cooling process. The slag mineralogy is dominated by hibonite, β-alumina, perovskite, calcium zirconate and F-Na-bearing calcium aluminate glass. Secondary minerals occur in close proximity to aluminum-calcium rich phases (hibonite, perovskite, gehlenite) and they were investigated in detail at the nanoscale using (S)TEM analyses and the results indicate that the secondary coatings are composed of a number of discrete phases. Whole-rock geochemical characterization demonstrates that Oka slag contains significant quantities of REE, U and Th. Bench scale leaching experiments were conducted using columns filled with crushed slag from the top, middle and bottom of the casts to investigate the mobility of U, Th, and REE in water draining from the slag. In general, the column effluent is characterized by high pH (maximum 13) and elevated Al (maximum 4906 mg/L) and F (704 mg/L). In the top sample, weathering of alumino-silicates and Al-rich glass resulted in high pH and elevated F^- concentrations, which rendered the slag from the top of the casts to be highly reactive, releasing high concentrations of Al, Ca, Na, and K and leading to the formation of mixed secondary amorphous Al/Ca hydroxide and barite ($BaSO_4$). The leaching and secondary-mineral properties of slag from the middle of the casts were similar, although aqueous concentrations in the leachate were slightly lower and secondary-minerals

included amorphous Si oxy-hydroxides. In general, leachate from the bottom of the slag casts displayed the lowest concentrations of major cations and the lowest reactivity. Secondary minerals were lesser abundant, but similar in composition to the top and middle of the casts except for the occurrence of Fe oxy-hydroxides resulting from weathering of ferri-gehlenite.

Acknowledgements

I would like to express my deepest appreciation to my supervisor Tom Al. His knowledge, understanding, positivity and spirit guided me through my time at the University of Ottawa. Working with Tom has given me the confidence and passion to pursue geochemistry. Thank you, Tom, for being a source of incredible encouragement and giving me opportunities to learn in a safe environment.

I am grateful to Jeanne Percival and Alexandre Desbarats at the GSC for their support and advice throughout my project. Their enthusiasm and curiosity encouraged me to development my own passion for research.

Thank you to Martin Couillard and Stephen Delahunty for their willingness to take time to explain and discuss results from (S)TEM data collection. I am very grateful for their support and interest in my project.

Thank you to the TERRE Network for opportunities to development my knowledge of mine site geochemistry as well as soft skills. The TERRE Network introduced me to an amazing community of researchers who have become important sources of support and friendship throughout my graduate studies.

I am very thankful to my fellow graduate students, whose energy kept me excited about research. In particular, a huge thank you to Lindsay Reynolds, Ayesha Landon-Browne, Karley Fugel, Evelyn Tennant and Ryan Miller for their help with my columns and for making my time at the University of Ottawa much better.

I would like to thank my parents and my sister for their unwavering love, encouragement and support along this journey.

Table of Contents

List of Figures

List of Tables

1 Introduction

This thesis reflects work conducted to characterize the weathering and leaching properties of slag from a niobium mine in Oka, Quebec. Chapters one to four cover the background, methodology, results, discussion, and conclusions of this characterization. Appendices A to F contain details of sample results and methodology in further detail.

1.1 Niobium Mining at Oka, Quebec

At present, the greatest use of Nb is in alloys, with the steel sector representing the premier consumer (Suri 2017; Simandl et al. 2018; Nagarajan, 2014). Although Nb has many uses its primary application is in the steel industry because of its low-temperature ductility, fabricability, and high temperature strength (Gupta and Suri, 1984). The second largest use is in nickel-based superalloys. The world's largest producers of Nb are Brazil and Canada (Simandl et al. 2018). The major Canadian deposits are in carbonatites at the former Oka and current St. Honoré, Quebec mines. The Oka deposit is located approximately 50 km west of Montreal, Quebec (Fig 1.) and it is hosted by a Cretaceous intrusive complex that is part of the Monteregian Hills province (Zurevinski and Mitchell, 2004). The Oka complex is a composite pluton of carbonatite rocks and silicate rocks (Gold et al., 1986). Rocks in the Oka complex can be divided into four series the first of which, carbonatites, is dominant. The carbonatite group is comprised of calcite carbonatite (sövite) with accessory amounts of apatite, biotite, melilite, monticellite, nepheline, niocalite, perovskite, pyrochlore, pyrite, pyrrhotite, richterite, sodian augite, strontianite, and witherite (Gold 1986). Other series in the complex include anoites and alnoite breccia, melteigite-urtite series, and okaite series (Gold 1986). In 1954, St. Lawrence

Columbium Group acquired mineral rights to a large area of the complex with the aim of exploiting commercial amounts of U (Carbonneau and Caron, 1965). However, the value of the Nb was soon recognized and it became apparent that it was more economically viable to extract Nb. A resource of Nb approximately 90 M tonnes at 0.4% Nb_2O_5 was outlined and Nb was produced from 1961 to 1977. With annual production of approximately 1.1 million kg of Nb_2O_5 in 1962 it was the largest producer of Nb in the world (Carbonneau and Caron, 1965).

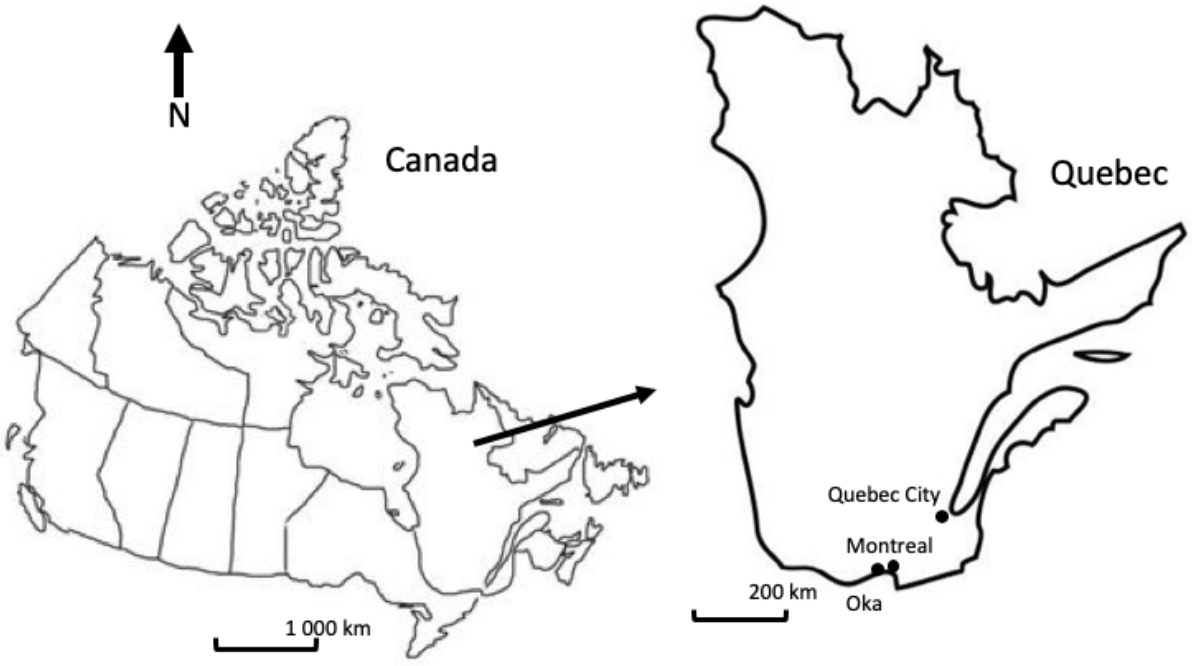

Figure 1. Location of Oka in relation to the city of Montreal, Quebec

At Oka underground mining operations began in 1965 with the construction of two open pits. A parallel circuit milling process was used to concentrate the pyrochlore into Nb_2O_5. In 1969, the company constructed a plant used for the smelting of ferroniobium. The smelting process at Oka relied on aluminothermic reduction. Aluminothermic reduction is a well-established method for producing ferroalloys that does not require heavy investment in terms of equipment or refinement (Suri 2017). The electrochemical potential of Al allows it to reduce

most oxides. In the aluminothermic reduction process Nb_2O_5 is mixed with Fe and Al and an exothermic reaction is initiated, releasing sufficient heat to keep the mixture molten (2200˚C) (Carbonneau and Caron, 1965) and drive the reactions to form Al oxides and ferroniobium as follows:

$3Nb_2O_5 + 10Al \rightarrow 6Nb + 5Al_2O_3$ (i)

$Fe_2O_3 + 2Al \rightarrow 2Fe + Al_2O_3$ (ii)

$Fe + Nb \rightarrow FeNb$ (iii)

While the mixture remains molten the heavier target metals segregate, sinking to the bottom of the melt. The target metals are tapped off from the bottom and the slag is then dumped into a pit formed from silica sand and allowed to cool.

1.2 General Properties of Slag

Slags are produced through the smelting process whereby pyrometallic raw ore is heated to extract desired metal. In general, slags are known for having low permeability thus have extensive applications in the cement industry. The average mineral grain size for slags varies based on their application from a micrometer to several hundred micrometers. Slags can be loosely divided into ferrous (steel and blast furnace Fe) and non-ferrous (Ag, Cu, Ni, Pb, Sn, Zn) slags.. The composition of ferrous slags are typically dominated by Ca and Si in the form of calcium-rich olivine group silicates ($(Ca, Mg, Fe)_2SiO_4$) and melilite-group silicates ($(Ca,Na)_2(Al,Mg,Fe^{2+})[(Al,Si)SiO_7)]$) that contain Al-, Mg- and Ca-oxide rich glass. Non-ferrous slags are dominated by Fe and Si with significant but lesser Al and Ca. Silicates in the olivine, and pyroxene are the dominant mineralogy of non-ferrous slag. Non-ferrous slags typically have a more negative impact on the environment when compared to ferrous slag based on trace element chemistry. However, trace element chemistry does not necessarily mean these

elements are released into the environment. Many leaching tests have been conducted in order to predict slag's impact on the environment (de Windt et al. 2011). Non-ferrous slag leachate has lower alkalinity and can sometimes produce acidity. Acidity can be produced by dissolution of sulphides such as pyrite:

$FeS_2 + 3.75O_2 + 3.5H_2O \rightarrow 2SO_4^{2-} + 4H^+ + Fe(OH)_3(s)$ (iv)

Iron and steel slags produce alkaline leachate from acid consuming reactions such as the dissolution of Ca oxides and silicates derived from compounds added as fluxing agents such as lime (Piatak et al. 2015). For example:

$CaO + H_2O \rightarrow Ca^{2+} + 2OH^-$ (v)

$Ca_2SiO_4 + 2H_2O \rightarrow 2Ca^{2+} + H_2SiO_4^{2-} + 2OH^-$ (vi)

Slags have commonly been considered inert during weathering because elements are incorporated in low solubility silicate and oxide crystalline frameworks (Piatak et al. 2015). However, slags are often enriched in toxic and radioactive elements and it is now known that they can be released into the environment through alteration processes and leaching (Piatak et al. 2015). Common secondary phases include iron oxyhydroxides, such as ferrihydrite ($Fe^{3+}{}_2O_3 \bullet 0.5(H_2O)$), goethite ($FeO(OH)$), and hematite ($Fe_2O_3$), as well as calcium sulfate ($CaSO_4$) (Piatak et al. 2015). Secondary silica, phosphate, hydroxide, carbonate or sulfate phases may host potentially toxic trace elements such as cadmium, chromium, and lead (Parsons et al. 2001; Piatak et al. 2015). The potential release of toxic and radioactive elements to the environment depends on the stability of all primary and secondary contaminant-bearing phases (Warchulski et al. 2015).

1.3 Oka Slag

Slags at the Oka site are located at the NW edge of the site (Fig. 2) and evidence of weathering is manifested by the occurrence of white precipitates along cracks (Fig. 3). Principal mineralogical components of the slag are hibonite ((Ca,REE)(Al,Ti,Mg)$_{12}$O$_{19}$), beta alumina ((Na,Mg,Sr,K)Al$_{11}$O$_{17}$), calcium zirconate (CaZr$_4$O$_9$), perovskite (REEAlO$_3$-CaTiO$_3$), and calcium aluminate glass (F,Na,Ce- CaAl$_2$O$_4$), with minor anorthitic plagioclase (CaAl$_2$Si$_2$O$_8$) in F-Na-REE bearing aluminosilicate glass (Fig. 4)(Mitchell and Mariano, 2016). Previous mineralogical investigation by Mitchell and Mariano 2016 indicates the presence of U- and Th- oxides in the calcium zirconate, perovskite, and anorthite bearing glass phases. Little is known about the chemical stability of slag from aluminothermic reduction of Nb, but perovskite is known to be unstable in low temperature groundwaters, and radiation damage in U- and Th- containing perovskites increases instability (Ringwood, 1991).

Figure 2. Satellite image showing location of slag at Oka mine site in 2018. Google Earth Image used.

Figure 3. Oka slag with white alteration product accumulated around cracks

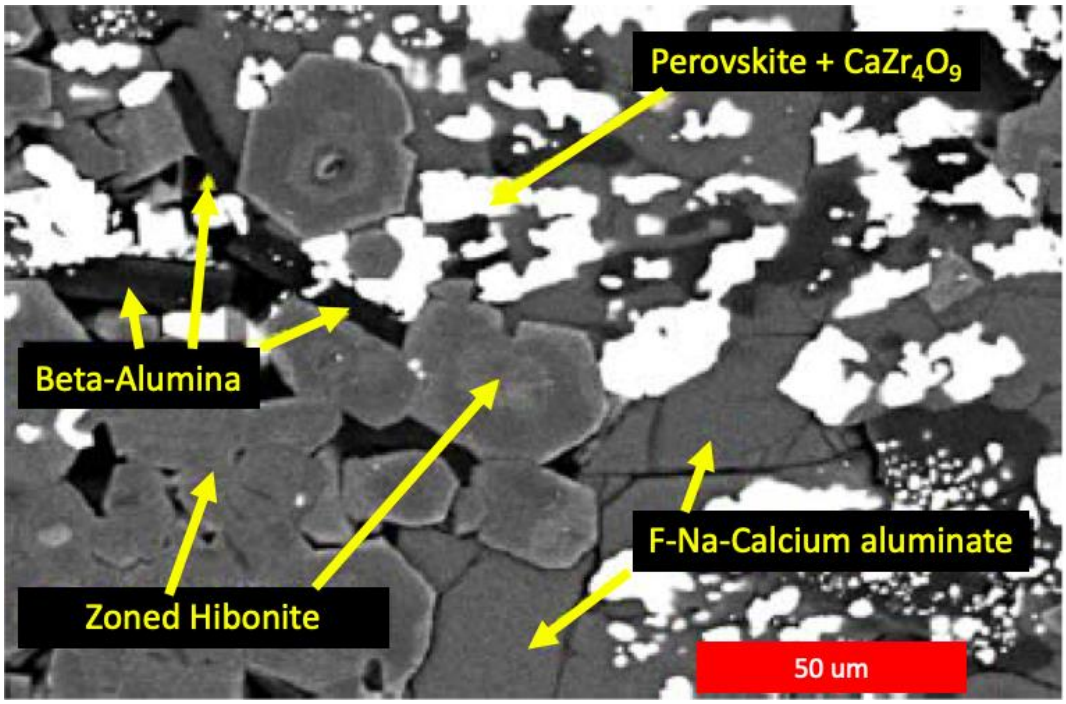

Figure 4. BSE image of Oka slag with zoned hibonite, Beta-alumina, perovskite and $CaZr_4O_9$. Modified after Mitchell and Mariano, 2016, Fig 13, p. 392.

1.4 Objectives

The objectives of this research are to investigate the weathering and leaching properties of Oka slag. This is done by characterizing the major and minor elemental compositions of leachate from the slag and by identifying secondary minerals that control the composition of the column leachate focusing on nanoscale reaction products. This work involves a column leaching experiment to simulate the weathering reactions and a detailed mineralogical analysis to understand the reaction products.

1.5 References

Carbonneau, C, and Caron, J. 1965. "The Production of Pyrochlore Concentrates at St. Lawrence Columbium and Metals Corp". *CIM trans.* 68: 71-79.

De Windt, L,, Chaurand, P, and Jerome Rose. 2011. "Kinetics of Steel Slag Leaching: Batch Tests and Modeling." *Waste Management*. 31(2): 225-235.

Gold, D.P., Eby, G.N, Bell, K, and Vallée, M. 1986. "Carbonatites, diatremes and ultra-alkaline rocks in the Oka area, Quebec." In Geological Association of Canada Guidebook; Geological Association of Canada..

A. K. Suri. 2017. "Extractive Metallurgy of Niobium." *Routledge*. 167-171.

C. K. Gupta. 1984. "Extractive Metallurgy of Niobium, Tantalum and Vanadium." *International Metals Reviews.* 29(1), 405-444.

Mitchell, Roger H. and Anthony N. Mariano. 2016. "Primary Phases in Aluminous Slags Produced by the Aluminothermic Reduction of Pyrochlore." *Mineralogical Magazine*. 80(2), 383-397.

Nagarajan, V. 2014. "Application of Niobium Microalloying in Heat Treatment of Engineering Steels." *International Heat Treatment and Surface Engineering*. 8(2), 80-85.

Parsons, Michael B., Dennis K. Bird, Marco T. Einaudi, and Charles N. Alpers. 2001. 2015 in text "Geochemical and Mineralogical Controls on Trace Element Release from the Penn Mine Base-Metal Slag Dump, California." *Applied Geochemistry*. 16(14), 1567-1593.

Piatak, Nadine M., Michael B. Parsons, and Robert R. Seal. 2015. "Characteristics and Environmental Aspects of Slag: A Review." *Applied Geochemistry*. 57, 236-263.

Ringwood, A. E. 1991 "Phase Transformations and Their Bearing on the Constitution and Dynamics of the Mantle." *Geochimica et Cosmochimica Acta*. 55(8), 2083-2110.

Simandl, G. J., R. O. Burt, D. L. Trueman, and S. Paradis. 2018. “Economic Geology Models 2. Tantalum and Niobium: Deposits, Resources, Exploration Methods and Market – A Primer for Geoscientists.” *Geoscience Canada*. 85-96.

Warchulski, R., A. Gawęda, M. Kądziołka-Gaweł, and K. Szopa. 2015. “Composition and Element Mobilization in Pyrometallurgical Slags from the Orzeł Biały Smelting Plant in the Bytom–Piekary Śląskie Area, Poland.” *Mineralogical Magazine*. 79(2), 459-483.

Zurevinskii, S. E. and Mitchell R. H. 2004. “Extreme compositional variation of pyrochlore-group minerals at the Oka carbonatite complex, Quebec: evidence of magma mixing?”. *The Canadian Mineralogist*. 42(4). 1159-1168.

2 Methods

2.1 Sample Collection and Geochemical Characterization

Full and partial casts of slag are discarded at the Oka mine site (Fig. 5). After aluminothermic reduction took place the slag was dumped into a slag pit to cool. In the slag pit these samples cooled at different rates based on a thermal gradient from the rim to the centre of the pit and a density gradient from the top to the bottom of the pit. This caused fractional crystallization and differentiation within the slag. Representative samples were collected according to anticipated differences related to fractional crystallization and differentiation within the slag while it cooled. Three samples were collected for the column experiment and 7 samples for the mineralogical investigation (Fig. 5). Sampling for mineralogy was focused on slag with visual evidence of alteration. Samples that were categorized as being from the "top" means that they cooled at the top area of the pit – these samples showed a ropey texture that was characteristic of slower cooling and likely would be less dense (Fig. 6). The samples characterized as being from the middle showed some ropey texture but also darker material with vesicles which are characteristic of a faster cooling environment and denser material (Fig. 7). Finally, the samples that were characterized as being from the "bottom" were dark with many vesicles which is characteristic of a denser sample that cooled rapidly (Fig. 8).

Figure 5. Discarded slag cast that cooled on the top of the slag – indicates slag cast diameter

Figure 6. Photo of the top of a slag cast

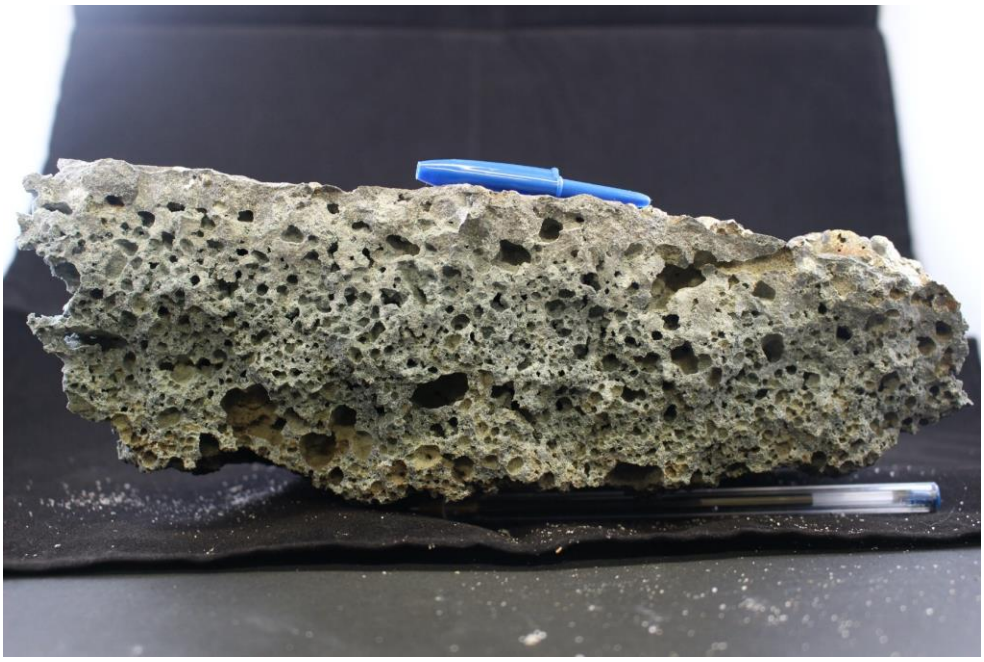

Figure 7. Sample collected representing "middle" of slag cast

Figure 8. In situ slag sample from "bottom" of slag cast

2.2 Lithogeochemistry

Samples were submitted to Actlabs for lithogeochemical analysis using lithium metaborate/tetraborate fusion, followed by whole rock and trace-element analysis by inductively coupled plasma optical emission spectroscopy (ICP-OES) and inductively coupled plasma mass spectroscopy (ICP-MS). No dilutions were made to the samples. Duplicates and Certified Reference Material (CRM) were used for QA/QC and results indicate this data is good quality (Appendix A, Table 6-8).

2.3 Column Experiments

Three columns were constructed from acrylonitrile-butadiene-styrene (ABS) pipe with an inner diameter of 5 cm and length of 25 cm. Nylon screens were placed at the bottom of each column to prevent loss of particulate material with the effluent. The slag samples were crushed and sieved with mesh between 40-100 μm and the columns were uniformly packed with crushed slag. A layer of felt was added at the top to evenly distribute the leaching solution which was a simulated precipitation (Table 1). Each day 2.13 mL of simulated rainfall were added to the column which is equivalent to 60% of the mean annual precipitation. Samples of leachate were collected for approximately 280 days with an average of 20 mL collected every 10 days. Although significant effort was used to replicate field leaching conditions the crushing of the slag increases exposed surface area to leaching. Thus, the results of this experiment might overestimate weathering rate of the slags.

Table 1. Composition of simulated precipitation based on aqueous concentrations recorded for rainfall at Frelighsburg, QC. in 2016 by Environment Canada

Ion	Concentration (mg/L)
SO4	0.90
NO3	1.49
Cl	0.20
Na	0.13
Ca	0.38
Mg	0.06
K	0.07

Leachate was analyzed for pH (Ross combination electrode, 8135BN), redox (Orion redox electrode, 9678BNWP), total alkalinity and phenolphthalein alkalinity (colourimetric titration using methyl-red bromocresol-green and phenolphthalein indicators). All redox measurements are referenced to the standard hydrogen electrode (E_h). Leachate samples were filtered (0.45 μm) and approximately 5 mL were filtered for analysis of anions (Cl, F, NO_3, SO_4, PO_4) by Ion Chromatography (IC; DIONEX-ICS-2100) and approximately 10 mL were filtered and acidified (trace-metal-grade nitric acid) for analysis of major cations and trace elements using (ICP-OES).

2.4 Mineralogy

2.4.1 X-ray Diffraction

All samples were pulverized in isopropyl alcohol using a McCrone micronizing mill, air dried and back-pressed into an aluminum holder. A Bruker D8 Advance Powder Diffractometer equipped with Lynx-Eye Detector was used with Co Kα radiation set at 35 kV and 35 mA. Diffraction patterns were collected using a Cu anode from 4.5˚ to 90.0˚ (2θ) using a step size of 0.02˚ and an integration time of 17. Identification of minerals was done using EVA (Bruker Nano Inc.) software with comparison to referenced mineral patterns using powder diffraction files

from the International Centre of Diffraction Data. Quantitative analysis was carried out using TOPAS (Bruker Nano Inc.) software.

2.4.2 Electron Microscopy and Microanalysis

Polished thin sections, 100-µm thick, were prepared at the University of New Brunswick of the 7 mineralogical samples for scanning electron microscopy (SEM). Grain mounts of the three column samples were also prepared at the University of New Brunswick. The SEM used is a JEOL 6610LV SEM equipped with an Oxford XMax SDD and energy dispersive X-ray spectrometry (EDS) detector running INCA (Oxford) analysis software. SEM-EDS was used to identify the principal mineral phases but the main focus was to locate secondary-mineral coatings on the grains and along fractures. The electron probe microanalyzer (EPMA) was used to quantify the elemental composition of primary and secondary minerals using JEOL 8230 Superprobe set at 1 nA and 15 kV. For each column 10 random areas on the grain mount were selected and mapped with EDS. Image size and resolution was changed for consistency and were processed using maxima with tolerance on ImageJ (Schindelin et al., 2012). Maxima with tolerance allows the user to set a maximum value and noise tolerance for a contiguous area and calculate a percentage of area above the maximum. Then a percentage based on maximum area of minerals were calculated.

Scanning transmission electron microscopy, ((S)TEM) combined with EDS and electron energy loss spectrometry (EELS) was used to further investigate fine-grained secondary minerals at the sub-µm scale. This work was conducted at two labs: the University of New Brunswick's Microscopy and Micro-analysis Facility using a JEOL 2011 (S)TEM equipped with a LaB_6 filament and operated at 200 kV and the National Research Council in Ottawa, ON using an

FEI Titan3 80−300 TEM operated at 300 keV and equipped with a CEOS aberration corrector for the probe forming lens and a monochromated field-emission gun to acquire annular dark-field (ADF) images (Fischione high-angle annular dark-field; HAADF detector). Locations for (S)TEM imaging and analysis were initially identified with the SEM, and then six samples were prepared from selected locations using a Focused Ion Beam (FIB) at Fibics Inc. following the method described by Patterson et al. (2002).

2.5 References

Patterson, R. J., D. Mayer, L. Weaver, and M. W. Phaneuf. 2002. "'H-Bar Lift-Out' and 'Plan-View Lift-Out':Robust, Re-Thinnable FIB-TEM Preparation for Ex-Situ Cross-Sectional and Plan-View FIB Specimen Preparation." *Microscopy and Microanalysis*. 8(S02). 566-567.

Schindelin, J.; Arganda-Carreras, I. and Frise, E. et al. (2012), "Fiji: an open-source platform for biological-image analysis", Nature methods 9(7): 676-682.

3 Results and Discussion

3.1 Lithogeochemistry

The bulk chemistry of the slag is dominated by Al_2O_3 (9.12-51.75 wt%), CaO (5.03-24.96 wt%) and SiO_2 (0.51-76.35 wt%) (Appendix A, Tables 3-6). However, SiO_2 concentrations were altered during the slag cooling in a silica-sand-lined pit resulting in contamination at the outer edges where samples contain high SiO_2 concentrations (71.68-76.35 wt%) (Fig. 6). The consistent high wt% of Al_2O_3 and CaO throughout the slag would classify these slags as ferrous slags. There were also high concentrations of some trace elements in the slag, particularly Nb (272 to >1000 ppm), U (17.5 to > 1000 ppm), Th (27.5 to >2000 ppm) and total Ce (over >3000 ppm). These concentrations were too high for measurements and therefore not fully quantified. Similar to the REEs, yttrium (Y) behaves as a moderately incompatible lithophile element in igneous systems (Cotten et al. 1995). Therefore, major oxides and trace element concentrations were plotted against Y as an index for chemical differentiation in the molten state (Fig. 7). Clear trends emerge showing variations in elemental concentrations in samples classified as from top, middle, and bottom; for example, incompatible elements such as U and Ba increase upwards whereas elements such as Fe and Mn that are compatible in the relatively dense mineral phases increase downward (Fig. 7). Examples of elevated concentrations for relatively incompatible elements near the top of the slag include Ba (1799 ppm), Ce (>3000 ppm), Dy (284 ppm), Er (94.3 ppm), Gd (383 ppm), La (>2000 ppm), Nb (> 1000 ppm), Nd (>2000 ppm), Pr (>1000 ppm), Sm (>1000 ppm), Sr (5434 ppm), Ta (>500), Th (> 2000 ppm), U (> 1000 ppm), Zr (> 10000 ppm). In general, top slags had the highest concentrations of large ion lithophile elements (LILE) and high field strength elements (HFSE). Elevated LILEs are found

in the top and middle samples because their large ionic radii causes them to behave incompatibly (generally considered with respect to mantle minerals) during fractional crystallization. The high ionic potential of HFSEs also causes them to remain in the melt and they too exhibit incompatible behaviour.

Figure 9. Mineralogical sample with silica contamination from the slag pit

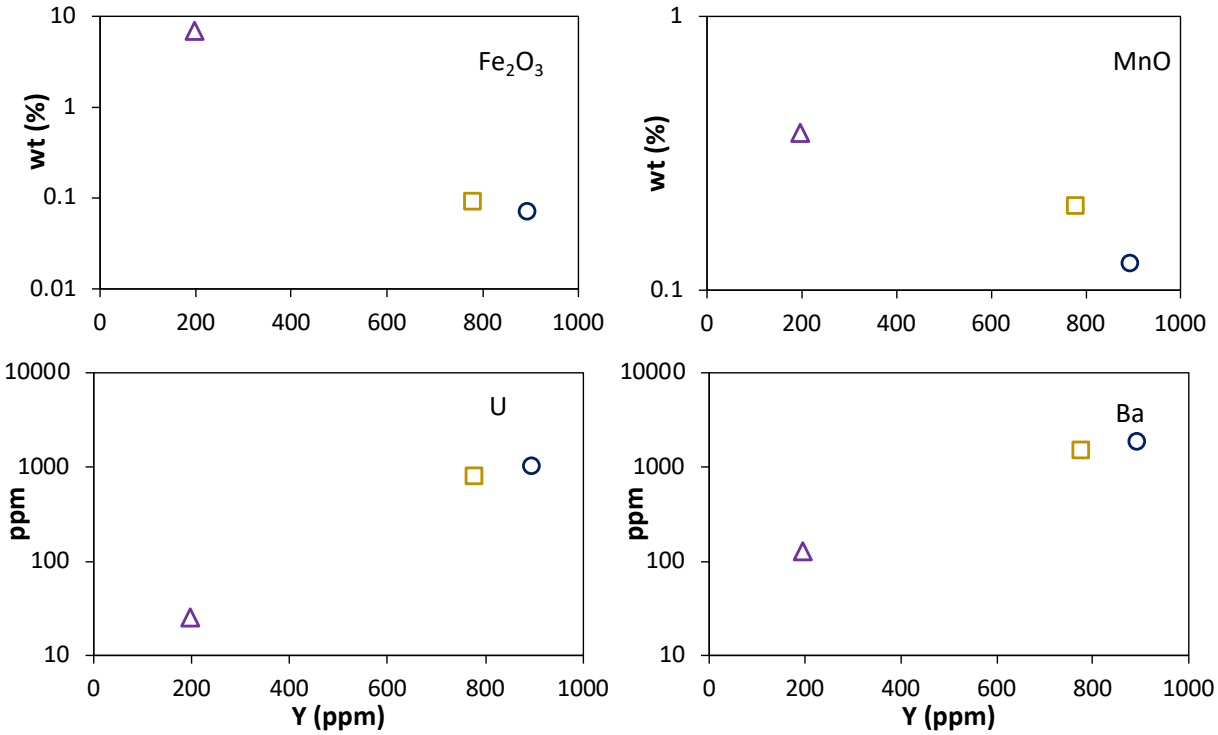

Figure 10. Samples of compositional variations in whole rock lithogeochemistry using Y as an index of chemical differentiation in the molten slag. Top, middle and bottom of the slag are represented by the circles (○), squares (□) and triangles (△) respectively

3.2 Column Experiment

` The effluent chemistry is plotted versus pore volume (PV) in Figure 8. Effluent from the top column is anomalous in that it displays the highest pH (10.97 - 13.25), alkalinity (181.9 - 3437 meq/kg), Al (40.02 - 4906 ppm), Ba (0.17 – 41.13 ppm), S (14.12 – 67.35 ppm), and F (4.1 - 704 ppm) and it has the lowest E_H (-339 - 278 mV; Fig. 8a). In the middle column, the effluent chemistry is similar in terms of pH (9.01 – 11.15), alkalinity (5.63 – 793 meq/kg), Al (0.53 – 260 ppm), Ba (0.14-21.97 ppm), S (0.40 – 44.52 ppm), F (0.314 - 8.98 ppm) and E_H (246 to 420 mV). The bottom column had the lowest pH (8.33 - 10.89), alkalinity (5.77 – 361 mg/L of HCO_3^-), Ba (0.01 – 1.00 ppm), S (0.74 – 14.42 ppm), and F (1.23 - 0.31 ppm). Elements of concern, such as U, Th and Ce where at detection limit values of 0.1, 0.5 and 0.1 ppb respectively.

The elevated pH of the column effluents is one of the most conspicuous features of the data. Ferrous slag leachates are reported to have high pH (up to 12.4) generated by dissolution of oxides of Ca, Mg, and the hydrolysis of calcium-alumino-silicate minerals (Piatak et al. 2015). Similar mechanisms are the most likely explanation for the high pH observed in the present experiments. In the top column, the very high pH values are associated with extremely high alkalinity due to the increased solubility of CO_2 at high pH and the prevalence of OH^-. In the columns, the confined pore space of the rock fragments causes CO_2 access to be limited by diffusion. A study by Hobson et al. 2018 found that during air-excluded leaching of ferrous slags, the dissolution of lime and calcium silicates resulted in high pH and high Ca leachate concentrations (Hobson et al. 2018). In contrast, an aerated leaching experiment showed lower alkalinity and Ca concentrations – these conditions are similar to the in-situ weathering of open fractures on the surface of slag fragments. In the same interval, the concentrations of Ca, Sr and Ba are relatively low, suggesting a carbonate solubility control on these elements. In the middle and bottom columns, the pH and alkalinity are relatively low, but the concentrations of Ca (middle and bottom), Sr and Ba (middle only) are elevated, which is also consistent with a carbonate solubility control. Unfortunately, geochemical modelling was not done on this system to determine the solubility controls because the code of choice, (PHREEQC; Parkhurst and Appelo, 2013) cannot account for non-carbonate (OH) alkalinity. However, with increasing PV, the concentrations of Ca in all three columns converge toward relatively constant values, possibly controlled by equilibrium with respect to calcite or fluorite. In the top and middle columns, the concentrations of Sr and Ba also converge to constant values, likely controlled by equilibrium with respect to their respective carbonate phases, strontianite and witherite,

respectively. The Sr and Ba concentrations in the effluent from the bottom column are lower by a factor of approximately 100, and they decline gradually, possibly as a result of surface passivation of the slag grains.

The concentrations of Al, Na and K are relatively high in the initial effluents from each of the columns, then declining gradually with increasing time (PV). The likely cause of these elevated concentrations is the dissolution of aluminate (and lower abundance aluminosilicate minerals) which are more soluble at high pH (de Windt, 2011). The high concentrations of Al, Na, K, and F found in the top column leachate can be explained by the weathering of interstitial F-Na-Ce aluminate glass and anorthite glass reported by Mitchell and Mariano (2016). The solubility of Al is elevated at high pH, but elevated Al concentrations may also be linked to the release of F to solution; Petrunic and Al (2005) reported F^- forms strong complexes with Al to enhance the dissolution of aluminosilicate minerals. It is expected that aqueous F^- leads to enhanced weathering as illustrated in Reaction vii:

$$CaAl_2Si_2O_8 + 6F^- + 6H^+ + 3H_2O + 2CO_2 \rightarrow Al_2Si_2O_5(OH)_4 + 2H_4SiO_4^0 + 2AlF_3^0 + 2CaCO_3 \quad \text{(vii)}$$

The elevated F concentrations in effluent from the top column coincide with relatively low Ca concentrations, suggesting that fluorite precipitation may represent an additional solubility limitation on Ca concentrations.

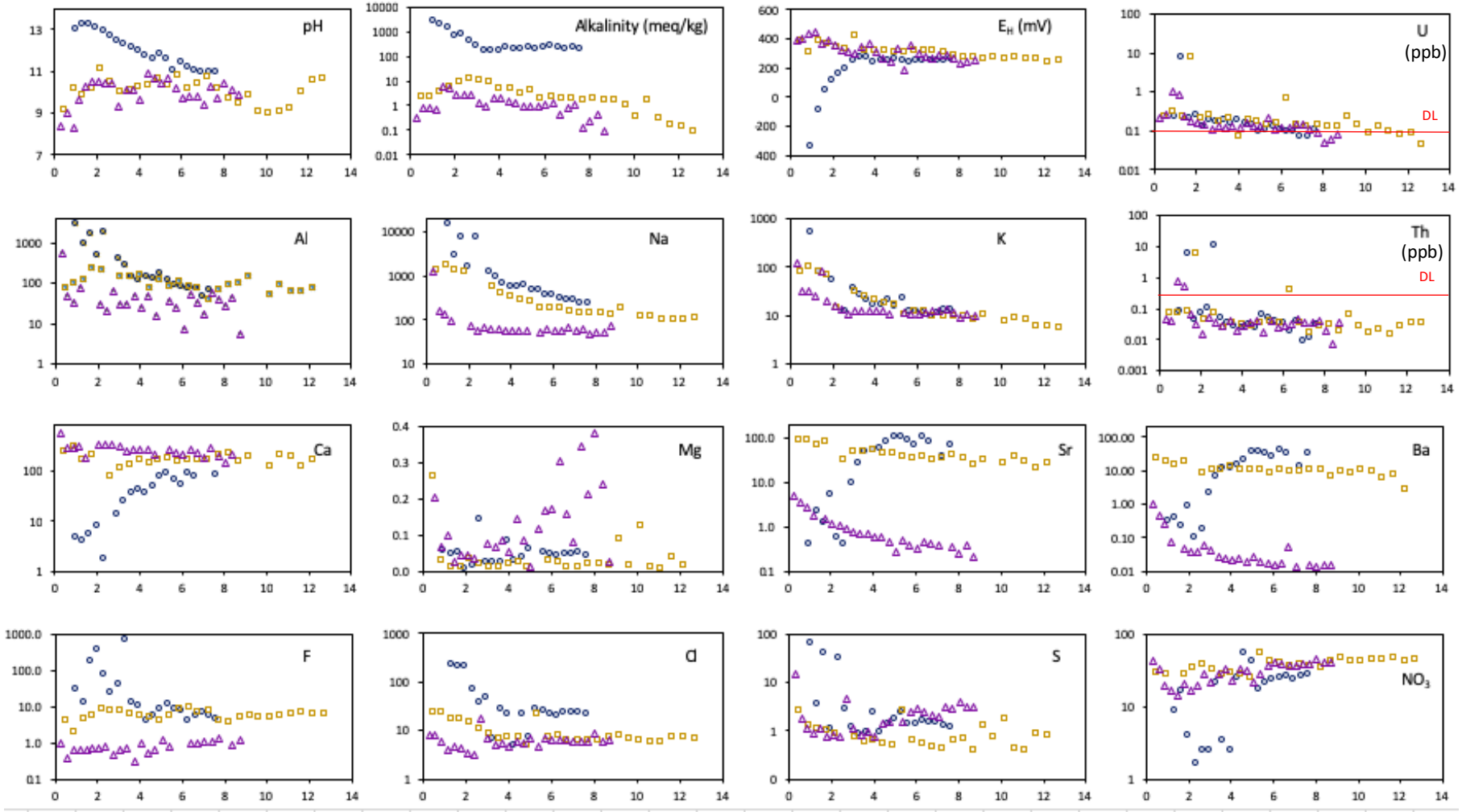

Figure 11. Aqueous geochemical data for effluent from the column experiments. All concentrations are reported in mg/L unless otherwise indicated and are plotted against pore volume. Columns for the top, middle and bottom of the slag are represented by the circles (○), squares (□) and triangles (△) respectively

3.3 Mineralogy

Powder X-ray diffraction indicates that the principal primary mineral phases are hibonite (11-59%), perovskite (non-detectable -35%), and gehlenite (non-detectable -31%) and grossite (8-23%) (Table 2, Appendix F). The large range in abundance for the main phases results from mineralogical zonation between the top, middle, and bottom of the slag. In a sample from the top, perovskite, hibonite, and grossite are the principal phases, along with significant quantities (8%) of fluorite (Table 2). In the middle, the dominant phases are perovskite, gibbsite, hibonite, and grossite. The bottom sample is distinct from the top and middle samples, with primary phases gehlenite, hercynite, grossite, anorthite and hibonite. All samples are similar in that they are composed of aluminum- and calcium-dominated minerals; a consequence of aluminum and lime addition during the smelting process.

Mineralogical investigations of thin sections using the SEM provide additional details of the primary mineralogy (Table 2), particularly for the abundance and distribution of amorphous phases. Similar to XRD, estimates from analysis of back-scattered electron images (BSEI) indicate that hibonite (0-58%), perovskite (0-23%) and gehlenite (0-15%) are the dominant primary minerals. However, ferri-gehlenite (0-27%), aluminosilicate glass (2-16%), beta alumina (3-8%), and calcium zirconate (0-7%) occur in minor amounts. Also similar to XRD, large variations in mineral abundance were noted from SEM data between top, middle, and bottom slags. Material from the top contains hibonite, perovskite, aluminosilicate glass, grossite, calcium zirconate, fluorite and beta alumina. Material from the middle has the same phases but in different proportions (Table 2). In the middle there is more hibonite and beta alumina but

less perovskite, grossite, and alimunosilicate glass relative to the top. Again, similar to the XRD results, SEM data indicate that slag from the bottom contains gehlenite, hercynite and anorthite, but ferri-gehlenite and minor columbite were also identified (Table 2).

The results of XRD and SEM investigations are generally consistent with the results of detailed examinations of the Oka slag by Mitchell and Mariano (2016). Mitchell and Mariano (2016) did not report mineralogical variations according to vertical position in the slag, but they report the occurrence of REE-, Th-, and U-bearing perovskite and calcium zirconate phases. The current mineralogical and U- and Th-whole-rock data demonstrate that these phases occur primarily in the middle and upper portions of the slags. Mitchell and Mariano (2016) also note that perovskite and beta-alumina host elevated concentrations of Ba and Sr. The present XRD and SEM investigations identified hercynite near the bottom of the slags which can account for the elevated concentrations of Fe and Mn observed in the whole rock data from the bottom. Mitchell and Mariano (2016) also reported Nb in a variety of complex oxide phases such as Fe-, Mn- and Mg-Columbite in the slag, leading them to comment that Nb separation was inefficient during the smelting process. In terms of slag reactivity, the abundance of F-bearing glass and fluorite near the top of the slag may be significant because the column-leaching data suggest that F^- enhances the weathering rates.

Table 2. Summary of primary mineralogy and their formulas

	XRD	SEM
Top	- 35% Perovskite - 30% Hibonite - 18% Grossite - 8% Fluorite	- 29% Hibonite - 23% Perovskite - 16% F-Na-Ce- Calcium Aluminosilicate glass - 15% Grossite - 7% Calcium Zirconate - 6% Fluorite - 3% Beta Alumina
Middle	- 59% Hibonite - 11% Gibbsite - 9% Perovskite - 8% Grossite	- 58% Hibonite - 10% Perovskite - 9% Grossite - 8% Beta Alumina - 6% F-Na-Ce- Ca Aluminosilicate glass - 6% Calcium Zirconate
Bottom	- 31% Gehlenite - 30% Hercynite - 23% Grossite - 8% Anorthite - 11% Hibonite	- 27% Ferri-Gehlenite - 22% Grossite - 16% Hercynite - 15% Gehlenite - 8% Anorthite - 3% Beta Alumina - 2% Columbite - 2% F-Na-Ce- Calcium Aluminosilicate glass

Mineral	Formula
Perovskite	- $REEAlO_3$-$CaTiO_3$
Hibonite	- $(Ca,REE)(Al,Ti,Mg)_{12}O_1$
Grossite	- $CaAl_4O_7$
Fluorite	- CaF_2
F-Na-Ce- Calcium Aluminosilicate glass	- F,Na,Ce,Ca- $Al_2Si_2O_8$
Calcium Zirconate	- $CaZr_4O_9$
Beta Alumina	- $(Na,Mg,Sr,K, Ba)Al_{11}O_{17}$
Gibbsite	- $Al(OH)_3$
Gehlenite	- $Ca_2(Al_2SiO_7)$
Ferri-Gehlenite	- $Ca_2Fe^{3+}AlSiO_7$
Hercynite	- $FeAl_2O_4$
Anorthite	- $CaAl_2Si_2O_8$
Columbite	- $(Fe,Mn)Nb_2O_6$

Secondary minerals formed by weathering of the slag are evident along cracks and fractures from the macro to the micro scale (Fig. 2, 12A-B). In general, SEM-EDS investigations indicate that secondary minerals are dominated by Al and Ca but compositional variations in the primary mineralogy affect the composition of the secondary minerals. Secondary minerals developed in samples near the upper surface of the slag display Al-rich regions (Fig. 12B), however, these regions are heterogeneous at the scale of several microns and below (Fig. 12C and D).

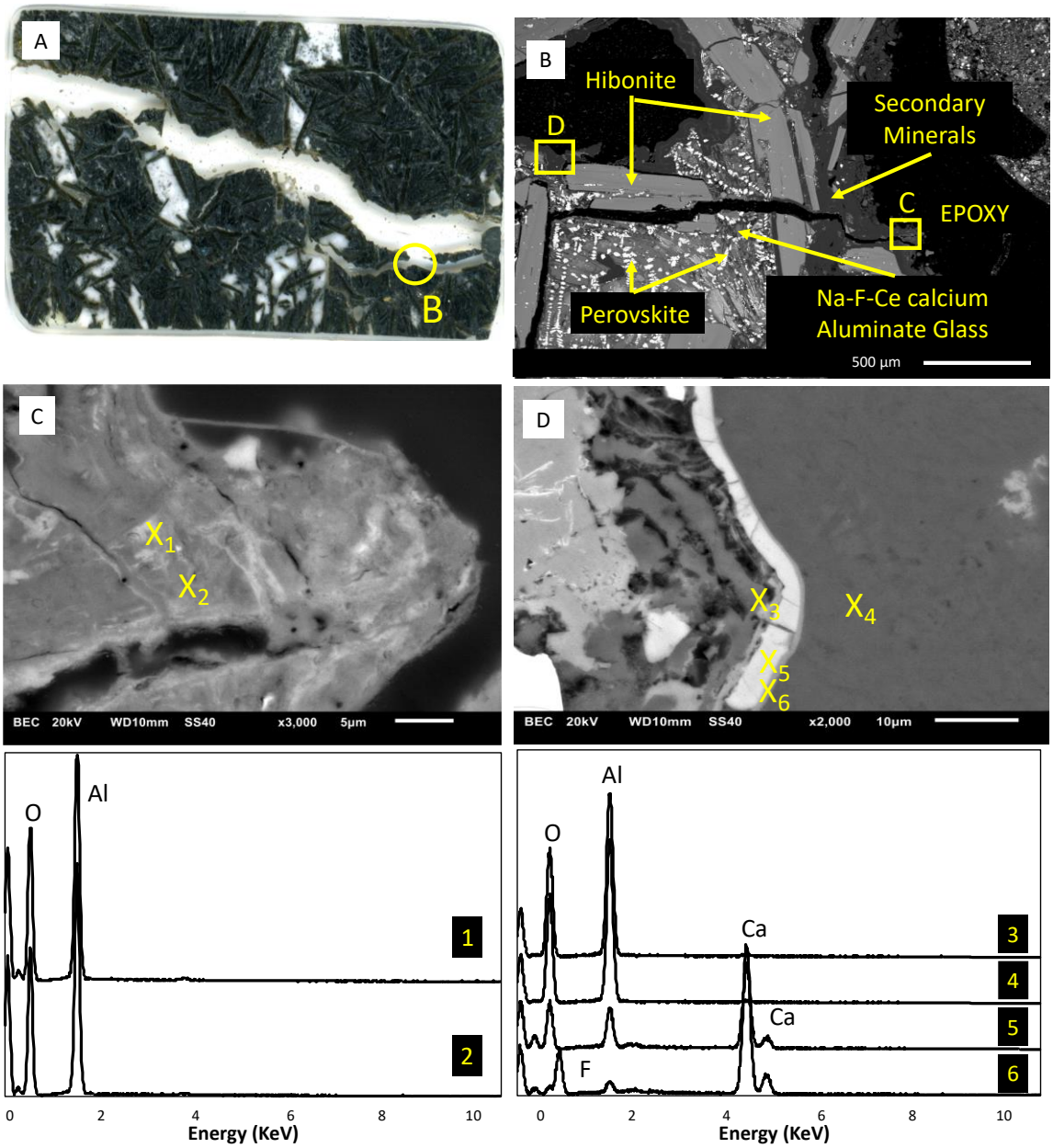

Figure 12. A) Scanned image of a polished thin section from the top of the slag; B) SEM BSE image showing primary minerals and spatial relationship with secondary minerals; C and D) higher magnification SEM BSE image of secondary minerals and locations of EDS spectra collection;1-6) EDS spectra from locations indicated on images C and D

A sample was prepared for (S)TEM analysis at the location indicated in Fig 13A. A low-magnification STEM image in Figure 13B shows the full width of the section. Visually, there are two distinct regions; a region with grey-white mottled contrast extending across the left-most

two thirds of the image, and a distinct grey vertical band near the right side which appears to be more homogeneous, possibly indicating a different composition. A closer investigation of the grey-white mottled region (Fig. 13C) indicates that it is composed of two phases, a spongey grey material is dominant and intergrown with lesser amounts of a dense white phase. STEM-EDS analyses indicate that the spongey-grey phase is dominantly composed of O, Al, Ca and F, probably fluorite intergrown with Al oxy-hydroxide, with lesser amounts of Sr, Na, K, Cl (Fig. 13-1 and 2). Broad diffuse rings observed in selected-area electron diffraction (SAED) patterns obtained from the O-Al-Ca-F material indicate that it is amorphous or nano-crystalline. The composition of the dense white phase is dominated by Ba, Sr and S (Fig. 13-1). This is likely barite or a Ba-Sr-SO_4 solid solution such as is common in seawater (Monnin and Cividini, 2006). Other areas on the same FIB section show similar compositional variations, including areas dominantly composed of O, Al, Ca and F and areas of Ba, Sr and S (Fig 14B-1 and 15B-1).

In the SEM BSEI shown in Figure 13D, secondary minerals occur in distinct banded zones, dominated by a broad Al-rich region on the right side, and narrow bands of Ca-O, Ca-F, Al-O rich material in the centre that separate the secondary phases from the primary minerals of the slag on the left side (Fig. 13D). A sample was prepared for TEM analysis from the region indicated in Figure 13D and a low magnification image of the section is shown in Figure 13E. At a low magnification, there is a band going through the centre of the TEM section separating the primary minerals on the right side from the secondary materials on the left. There appears to be four distinct regions within the secondary materials. STEM-EDS analyses indicate a Ca-O phase (Fig 13-6). This Ca-O phase is preceded by a fairly homogenous material with dislocations (Fig. 13F). STEM-EDS analyses indicate this material is an Al-O phase (Fig. 13-5). Based on SAED

patterns this Al-O phase is nanocrystalline. However, in contrast to the material represented by the analysis in Fig. 13-4 SAED data indicates that it is an amorphous phase while STEM-EDS indicates it is a homogeneous Ca-F phase. The final section from the top appears heterogeneous and mottled with a higher porosity. STEM-EDS indicates this section is an Al-O phase, however, the heterogeneity within this area visible in Fig. 13G indicates there is likely another unresolved phases present. The higher porosity and amorphous nature of this phase indicates that the Al is likely in the form of a hydroxide or oxyhydroxide. A closer look at the material in Fig. 13E outlined by the box can be seen in Fig. 13G. This secondary material has a high porosity and is Al-rich consisting of Al-O and Al-Ca (Fig. 13-7). Similar to Fig. 13C, Fig. 13G has an Al-Ca-O phase accompanied by minor Ba and Sr. The heterogeneities seen in the Al-Ca-O and Al-O phases are likely a result of the minor Ba and S. Unfortunately, the extremely high porosity of these areas made them difficult to analyze with the (S)TEM because they are sensitive to beam damage.

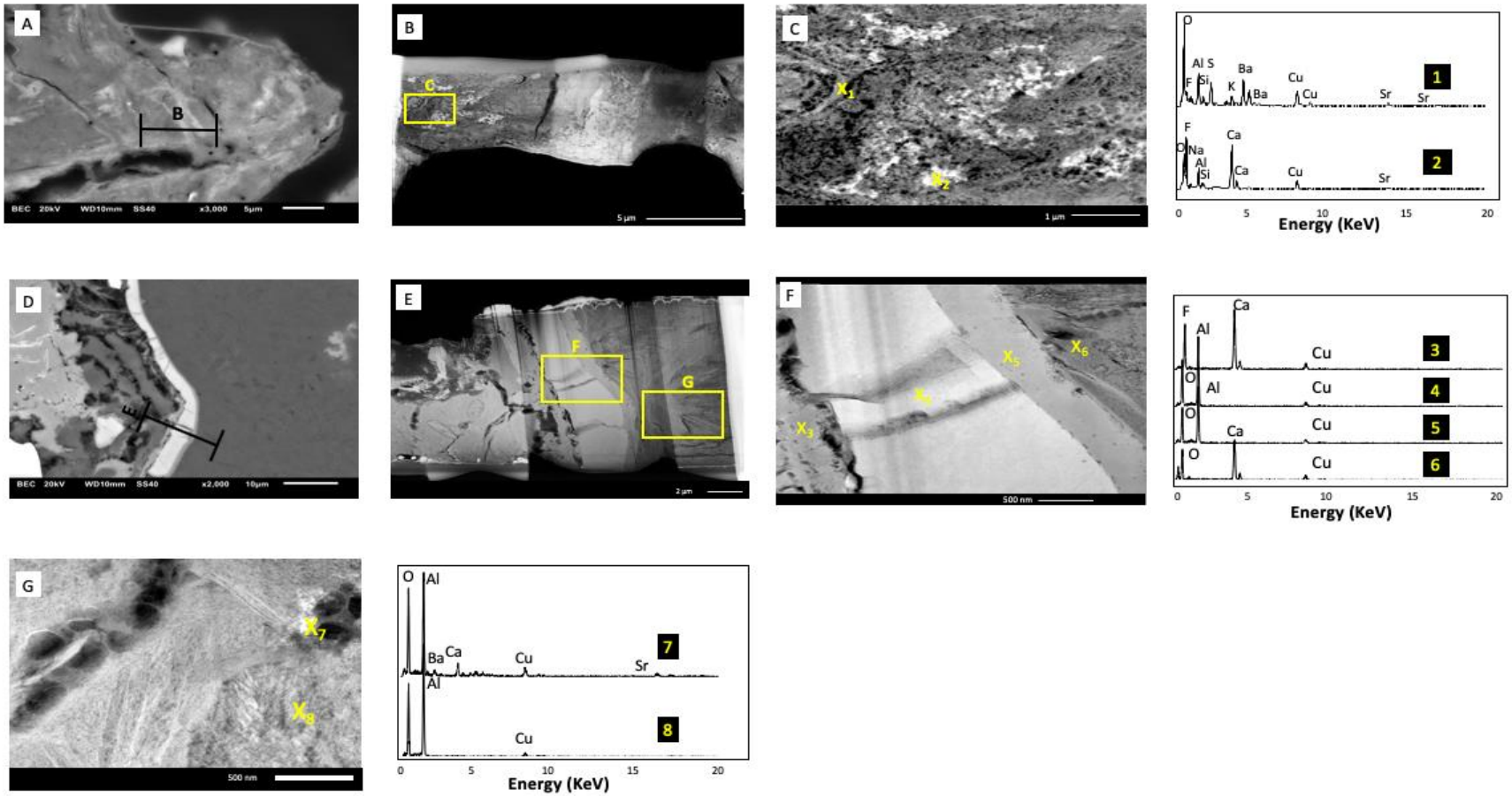

Figure 13. A) High magnification SEM-BSE image of area labelled C on figure 12-B B) STEM-HAADF image of FIB section cut from the location indicated on image A; C) higher magnification STEM-HAADF image of the region of interest indicated on image B 1-2) STEM-EDS spectra from areas indicated on image C. D) High magnification SEM-BSE image of area labelled D on figure 12-B E) STEM-HAADF image of entire FIB section; F) Higher magnification STEM-HAADF image of banded area in the region of interest indicated on image E; 3-6) STEM-EDS spectra from areas location on image F. G) High magnification STEM image of area labelled G located on E 7-8) STEM-EDS from points indicated on image G.

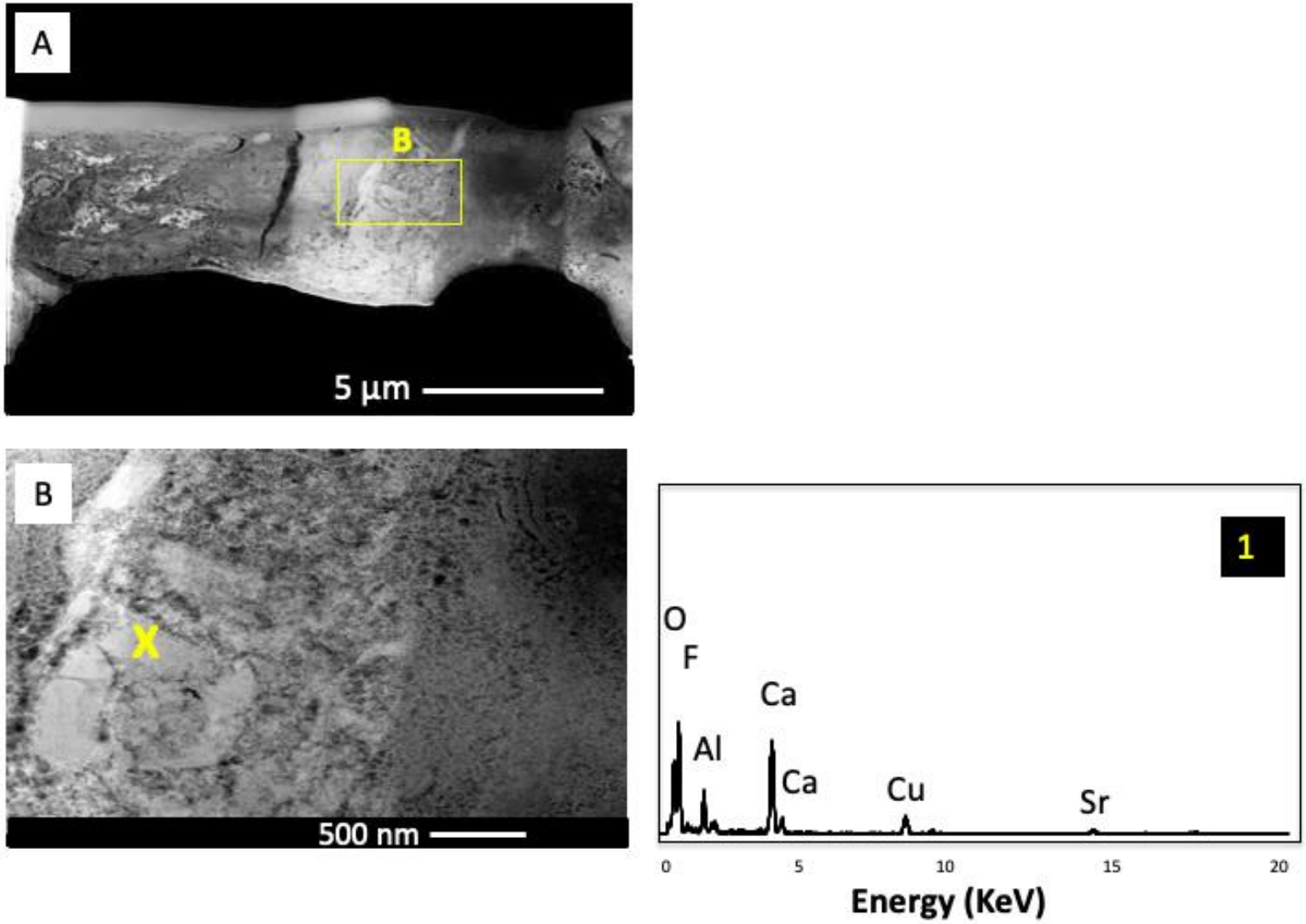

Figure 14. A) STEM-HAADF image of FIB section cut from the location indicated on Fig 13A B) higher magnification STEM-HAADF image of region of interest indicated on image A 1) STEM-EDS spectra for areas indicated on image C.

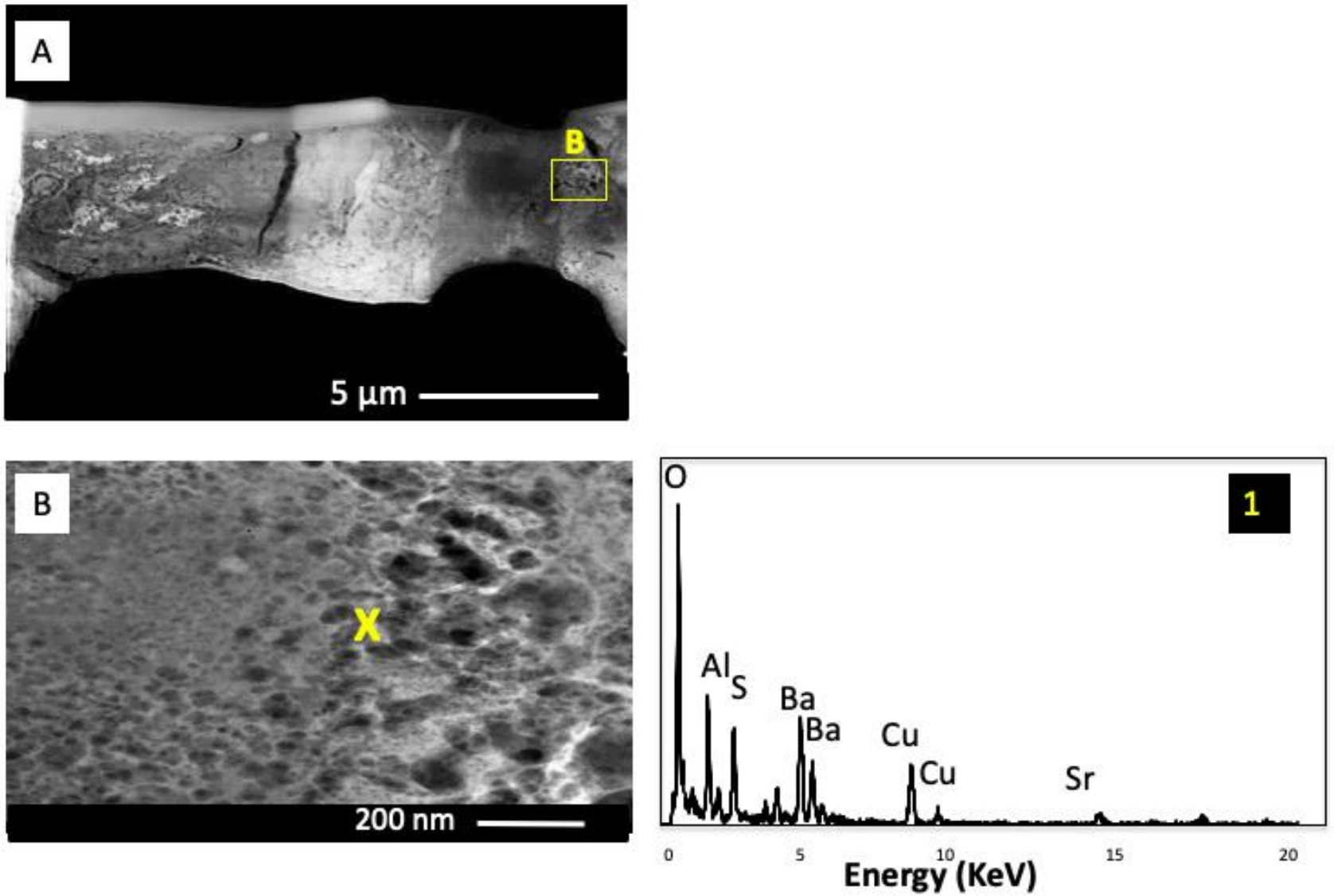

Figure 15. A) STEM-HAADF image of FIB section cut from the location indicated on Fig 13A B) higher magnification STEM-HAADF image of region of interested indicated on image A 1) STEM-EDS spectra for areas indicated on image C.

In the middle sample there are holes within the thin section which could be evidence of dissolution. These cracks are indicative of secondary material as coatings on fractures and cracks in the slag (Fig. 16B). Areas such as this were the focus of SEM-EDS point analyses in order to identify secondary precipitates. At the micrometer scale identification of primary minerals and their secondary coatings was possible (Fig. 16C). SEM-BSE of these secondary coatings indicate compositional variations within the material and that material composition is different at each location. An Al-O phase is abundant in the secondary material as well as an Al-Si phase which is dominant closer to the primary minerals. The phase close to the edge of the secondary precipitate is a Ca-rich phase. Whether these three phases are homogeneous is not clear at this scale, although variations in the SEM-BSE image indicate that there could be heterogeneities. Furthermore, these phases could determine how the primary minerals are weathering over time based on their spatial relationship to the primary minerals.

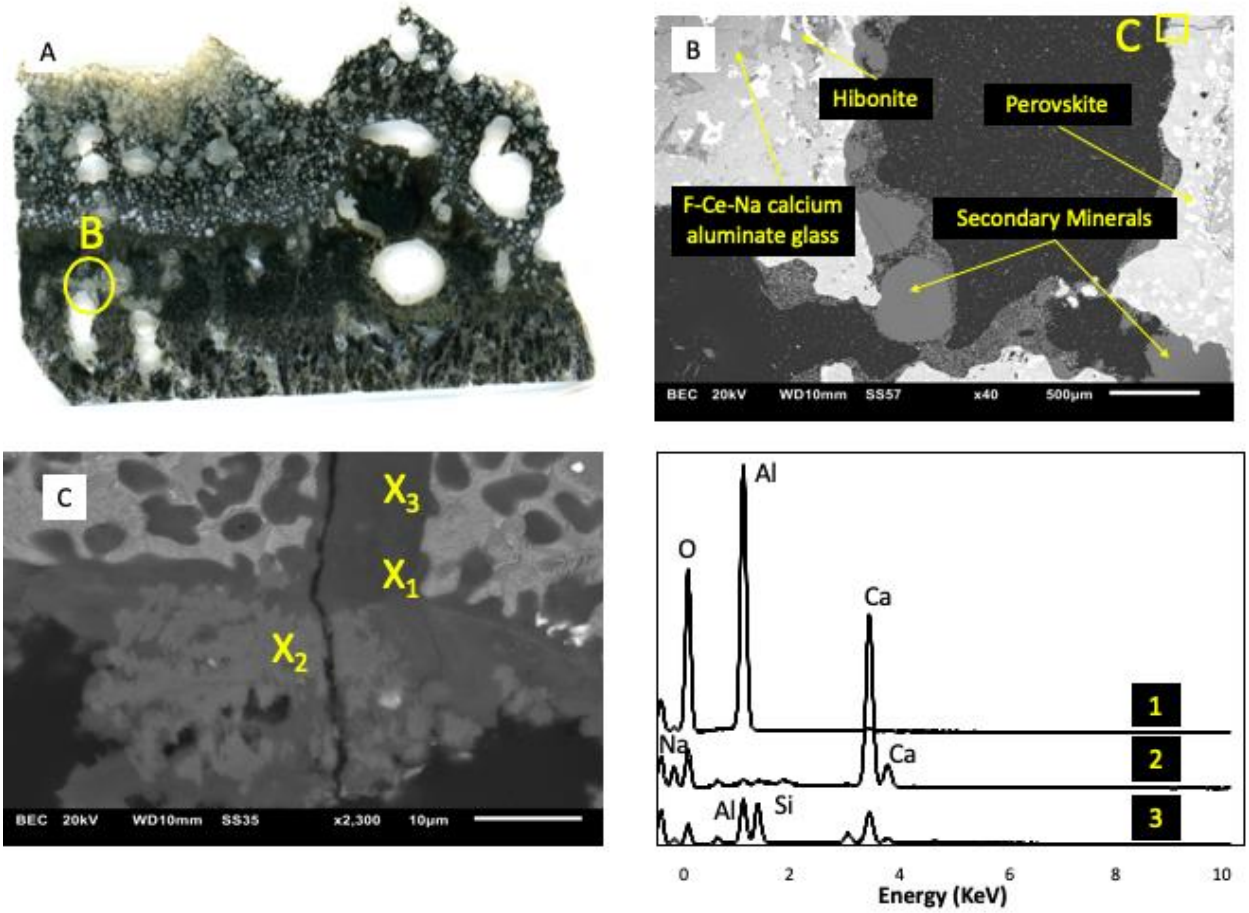

Figure 16. A) Scanned image of a polished thin section from the middle of the slag; B) SEM BSE image showing primary minerals and spatial relationship with secondary minerals; C) higher magnification SEM BSE image of secondary minerals and the area where TEM sections were cut by FIB; 1-3) SEM-EDS spectra from locations indicated on image C

A sample was prepared for (S)TEM analysis at the location labelled B on Figure 17A. Figure 17B shows a low magnification STEM image of the full width of the section. From this low magnification STEM image there are three distinct regions within the secondary material. The first is a dark grey porous material that appears to be homogeneous and occurs on the right side of the section, extending into a sharp angled contact with the second region of lighter grey. A higher magnification view of the dark grey region indicates it is porous, but apparently homogeneous (Fig. 17C, right side), and STEM-EDS analyses indicate that it is composed of Al-O

(Fig 17-4). The lighter grey zone in the middle of the TEM section has a less porous texture and the grey-white mottled appearance suggests greater heterogeneity (Fig 17C, left side). STEM-EDS analyses indicate that this region contains mixed nanoscale phases (Al-Si-K-Ca-O, Ca-C-O and Al-Si-Ca-O; Fig 17-1 and 2). Another region on the same FIB section shows similar compositional variations such as Al-O (Fig 18-1), Al-Si Ca-O (Fig 18-2) and Al-Si-K-Ca-O (Fig 18-3).

Another (S)TEM sample was prepared from location C as indicated on Fig 17A. This sample was made closer to the primary material than location B. This was done in order to link chemical variations to spatial relationship with primary minerals. In the STEM image the bright mineral is perovskite which has been infilled with F-Na-Ce-Ca-aluminosilicate glass, both of which would have formed during the smelting process (Fig. 157. The secondary material is the dark grey zone along the left side of Figure 17C, next to the perovskite and the F-Na-Ce-Ca aluminosilicate glass. Based on this secondary material's spatial relationship with the primary minerals it is likely that these secondary minerals are less developed than the secondary minerals in Figure 17B and D. A higher magnification STEM image shows the boundary between the primary and secondary minerals. In this sample the secondary material appears homogeneous and porous. STEM-EDS analysis indicates that it is an Al-O phase with traces of Na and Ca (Fig. 17-5)

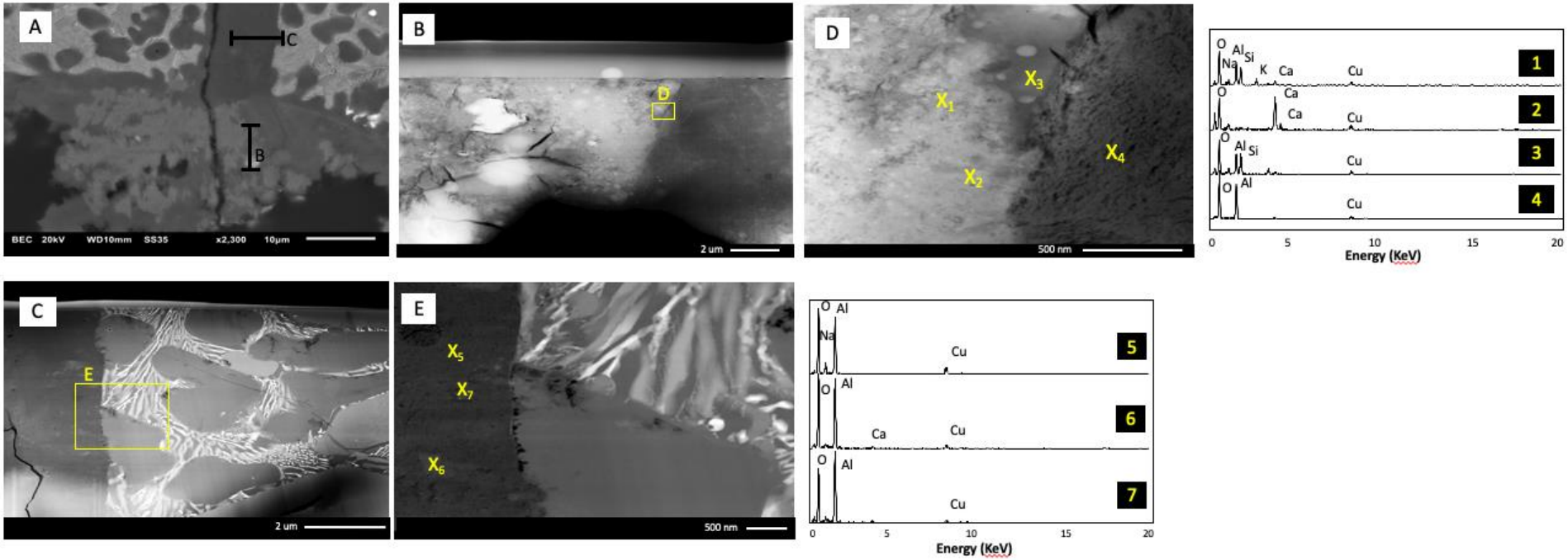

Figure 17. A) SEM-BSE image of area labelled C located on Fig 16B.B) STEM-HAADF image of FIB section cut from location B indicated on image A; C) STEM-HAADF image of FIB section cut from location C indicated on image A D) Higher magnification STEM-HAADF image of region of interested indicated on image B 1-4) STEM-EDS spectra from locations indicated on image D. E) Higher magnification STEM-HAADF image of region of interest labelled E indicated on image C; 5-7) STEM EDS spectra from locations indicated on image E

.

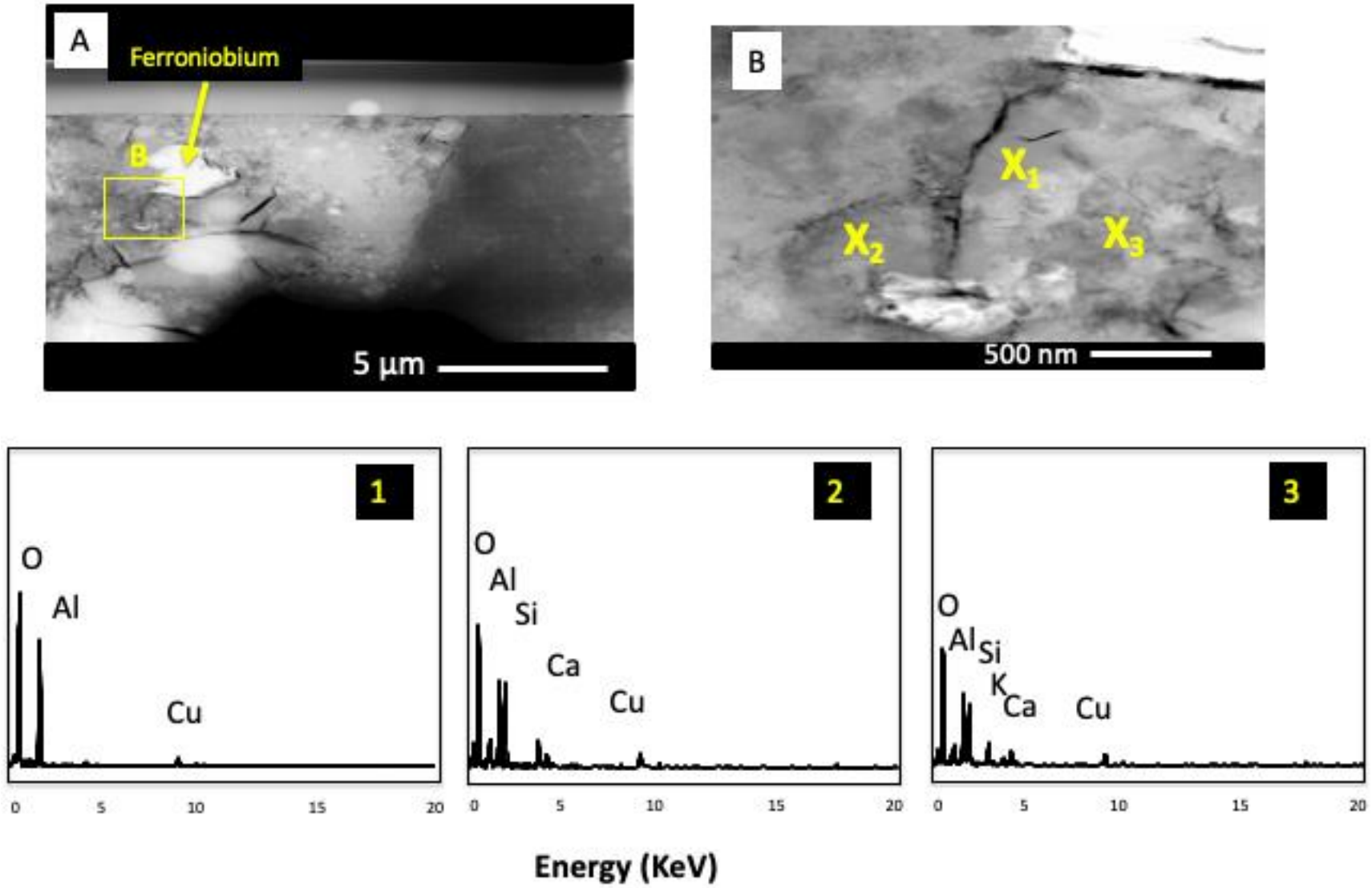

Figure 18. A) STEM-HAADF image of FIB section cut from location 17A labelled B B) higher magnification STEM-HAADF image of the region of interested indicated on image A 1-3) STEM-EDS spectra from the locations indicated on image B.

The secondary minerals observed in the bottom sample differs from that of the top and middle samples. Secondary minerals were not visible at the macro scale, however, investigations with SEM-EDS identified secondary minerals as coatings encapsulating gehlenite grains. In BSE images, the coatings appear to be heterogeneous with bright and dark regions evident (Fig. 19A). SEM-EDS analyses at point locations indicate that dark regions are primarily composed of Al and Si (Fig. 19-1). Analysis of the bright regions was limited by the spatial resolution of the SEM, but results suggested these areas contain Fe. A section was prepared for (S)TEM to achieve higher resolution for analysis.

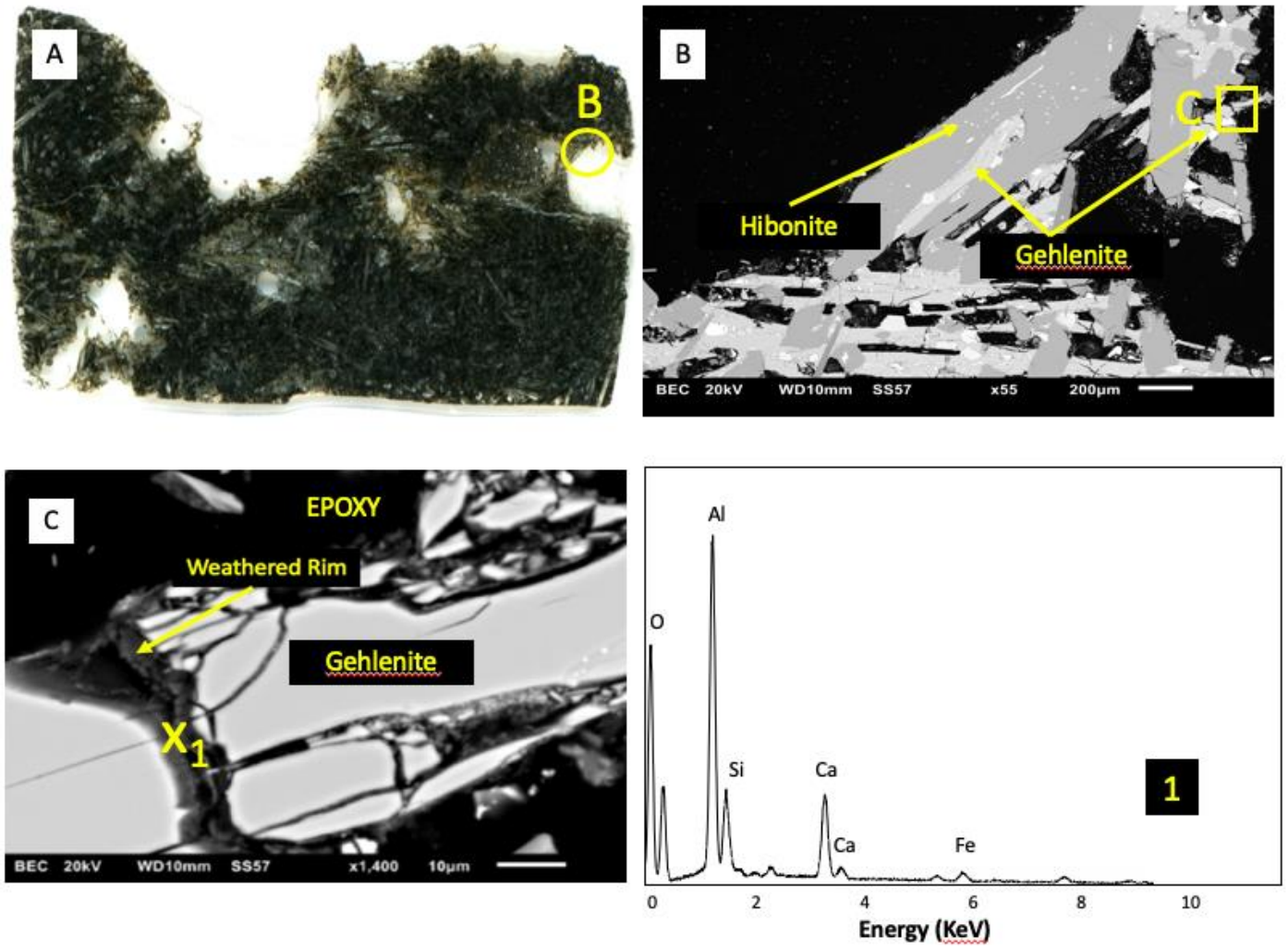

Figure 19. A) Scanned image of a polished thin section from the bottom of the slag; B) SEM BSE image showing primary minerals and the location of weathered gehlenite; C) Higher magnification SEM BSE image of gehlenite showing a weathered rim; 1) EDS spectrum from location indicated on image C

;

The section was prepared, extending from the gehlenite grain to the edge of the secondary material (Fig. 20A). A STEM image of the sample at low magnification shows the width of the section and the presence of an abrupt boundary between the gehlenite grain and the secondary minerals (Fig. 20B). At this scale there appears to be two distinct regions; a grey-white region with mottled layers parallel to the gehlenite grain and a distinct bright rim at the outer edge of the weathered rim. STEM-EDS analyses indicates that the layered grey phase is

composed of O, Al, Si with trace amounts of Ca and Fe (Fig. 20-1 to 3). An EELS line scan (Fig. 20C-4 to 5) indicates that the Ca content of the coating is low and decreases with distance from the gehlenite grain, suggesting that Ca has been removed by the weathering reaction. In contrast, the coating contains Fe and Mn which increase in abundance with distance from the gehlinite grain. Selected-area electron diffraction (SAED) patterns obtained from this material indicate that it is amorphous or nano-crystalline. The composition of the white phase on the outer edge is similar to the O-Al-Si coating but contains a relatively high abundance of Fe. Amorphous Al-Si and/or Fe-Mn coatings on aluminosilicates in other steel slag leaching studies have been reported by Hudson-Edwards et al. 1999, Meima and Comans. 1999, De Windt et al. 2011 and Piatak et al. 2015.

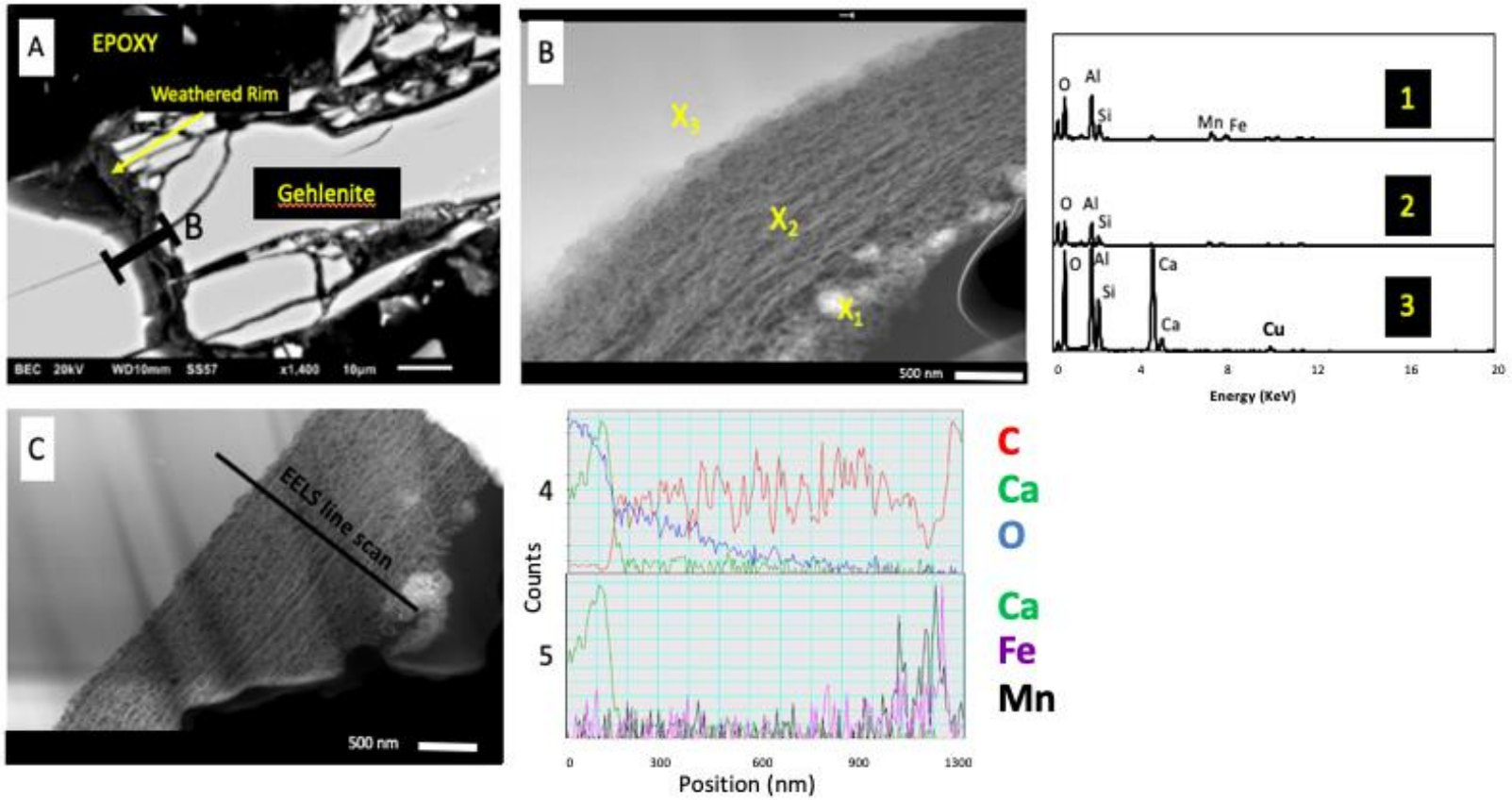

Figure 20. A) SEM-BSE of area C in image 19B B) Higher magnification STEM-HAADF image at the boundary between gehlenite and the weathered rim; 1-3) STEM-EDS spectra from areas indicated on image B; C) STEM-HAADF image of weathered gehlenite rim showing the location of the EELS line scan; 4-5) EELS line scan showing relative abundance of C, Ca, O, Fe and Mn.

Overall, the secondary minerals in the top samples are predominantly Al and Ca hydroxides. Dissolution of silicates and subsequent reactions to form hydroxide secondary minerals has been well reported in ferrous slags (Piatak et al. 2015). Results from top samples of the Oka slag are consistent with other studies, which have identified Al- and/or Ca- hydroxide coatings as weathering products of ferrous slags (Piatak et al. 2015, Warchulski et al. 2015). A secondary fluorite (CaF_2) and a Ba-Sr-SO_4 solid-solution have also been identified in the top sample. Strontium is the most common impurity in barite and studies indicate the Ba-Sr-SO_4 solid solution is likely to form given the extremely low solubility of barite (Monnin & Cividini. 2006). The mechanism for formation of the Ba-Sr-SO_4 solid solution would be the co-precipitation of Sr with barite (Monnin & Cividini. 2006). Sulfates of Ba, Ca, Cu, Fe, Mg, and Pb have been reported in slags but occur more commonly in non-ferrous slag formed following the dissolution of sulfides (Piatak et al. 2015). In addition to limiting aqueous Al, Ca, and F concentrations in leachate, the O-Al-Ca-F precipitate provides a mineralogical control on the aqueous concentrations of Na and K. There are a number of possible sources for the elements contained in these secondary minerals. Aluminum, Ca, Na and F could be from dissolution of fluorite and F-Na-Ce-Ca-aluminate glass, and weathering of beta alumina would release Sr, Ba, Na and K. Spatially, phases such as beta alumina and F-Na-Ce-Ca-aluminate glass coincide with the presence of these secondary minerals.

Effluent chemistry from the top column provides evidence towards the weathering of F-Na-Ce-Ca-aluminate glass. The high concentrations of Al, Na, and K in initial effluent likely coincide with the weathering of the F-Na-Ce-Ca-aluminate glass. Low concentrations of REEs, U, and Th in effluent and the absence of REE, U, or Th bearing secondary minerals in the

weathered product indicates perovskite and hibonite are likely not weathering. The higher reactivity reported in the top column is likely based on the enhanced solubility of the amorphous F-Na-Ce-Ca-aluminate glass. The release of calcium was likely an effect of hydration and carbonation of CaO(lime) and release of Ca and its hydrates in contact with the simulated precipitation. Tossavainen 2005 compared different types of slags and concluded that there are faster releases of calcium and aluminum in slowly cooling slags. This indicates that the top samples would tend to be more reactive in comparison to the bottom samples. The high alkalinity paired with the high pH indicates high OH^- in effluent. Effluent chemistry in the top column is similar to effluent of blast furnace slags in terms of pH and alkalinity. Such leachates are generated by the dissolved of oxides of calcium, aluminum and magnesium. Slags of this nature can produce hydraulic slag cement dominated by calcium silicate hydrates and calcium aluminate hydrates which could explain the Al and Ca hydroxides noted in EDS analysis (Glasser, 1992). However, these types of cement forming reactions may hamper evaluations of leaching results and should be considered (Tossavainen 2005).

Although elements of concern are not being mobilized at this time in the top column the high pH, high alkalinity, and high Al concentrations bring forward the most significant environmental concerns based on drinking water concerns for aesthetic or provisional guidelines. There is also a concern about high pH and calcium loadings in leachate resulting in high calcium carbonate precipitation upon contact with atmospheric CO_2 which can smother benthic communities (Piatak et al. 2019).

The secondary mineralogy of the middle sample is subtly different from that of the top samples. The secondary minerals are predominately Al and Ca hydroxides and their nature is

consistent with the weathering of aluminosilicates which has been explored in a number of ferrous slags (Piatak et al. 2015). However, the secondary mineralogy from the middle of the Oka slag includes Al-Ca-Si phases which provide a mineralogical control on the Al, Ca, and Si concentrations as well as Na and K. The primary mineralogy of the middle sample is subtly different than that of the top, which explains the similarities in the secondary mineralogy. The source of these products is uncertain; however, Al-Ca-Si could be a product of aluminosilicate glass dissolution. This is likely because aluminosilicate glass is also one of the main sources of Na in the slag.

The effluent chemistry from the middle sample shows lower leaching rates when compared to the top samples. Lower concentrations of Al, Ca, K, and Na paired with lower alkalinity and pH are indicators of lower reactivity in the middle sample. The dominance of Al-Ca-Si as secondary products explains lower concentrations of Al and Ca in effluent. The formation of this secondary product coincides with research on steel slags (Piatak et al. 2019).

The lower reactivity of this sample is likely attributed to the primary mineralogy where there is less of the soluble amorphous F-Na-Ce-Ca-aluminate glass. Similar to the top column, it's likely that the F-Na-Ce-Ca-aluminate glass is weathering to produce these secondary minerals. However, this glass is only 6% of the primary mineralogy of the middle sample. There are also lower concentrations of Al and Ca in the lithogeochemistry of the sample. This is likely a result of the abundance of Hibonite (58-59%) in the middle sample. The prevalence of Ca and Al silicates and hydroxides as secondary minerals is indicating that the dissociation of Ca and Al hydroxides to form their component ions and release hydroxide ion will increase the pH. This explains the pH-Al-Ca-alkalinity correlations noted in the effluent chemistry.

Similar to the top sample elements of concern are not being mobilized, however, the high pH, alkalinity and Al concentrations may be a significant environmental concern based on aesthetic and provisional drinking water guidelines. Comparatively, the effluent quality of the middle sample is better than the top sample in terms of pH, alkalinity, and Al concentrations.

In the bottom sample secondary mineralogy is Al-Si dominant with lesser amounts of Fe and Mn. Precipitation of the Al-Si-Fe-Mn coating likely controls the leachate concentrations of Al and Fe. The layered appearance of the coating parallel to the gehlenite grain boundary indicates that the Al-Si coating precipitates along the boundary as weathering proceeds. The Al-Si coating is porous at the nanoscale. Precipitation of Fe oxyhydroxides at the edge of the coating suggests incongruent dissolution of ferri-gehlenite with the formation of Fe-oxyhydroxides first followed by the gradual formation of Al and Si variable precipitates.
At elevated pH, there are potential issues with high concentrations of some metals and metalloids; notably those which form oxyanions and are mobile under alkaline conditions.

The dominance of Fe-Ca-Al silicates within the primary mineralogy of this slags distinguishes it from the top and middle slags. These silicates are weathering at a slower rate because of the absence of aluminosilicate glass providing fluoride (reaction vii). However, there is indication of weathering forming Al-Si precipitates and Fe oxyhydroxides. Lower pH and lower alkalinity indicate lower reactivity and likely a different mechanism controlling the high pH. Ferrous slags generally produce alkaline leachate through the dissolution of Al/Ca silicates and oxides. In this situation the presence of gehlenite is likely reacting with water to form the secondary aluminum rich silicates, Ca and produce OH^-. This reaction would be similar to the weathering of anorthite to kaolinite clay. The weathering of ferri-gehlenite to produce Al

silicates would explain why concentrations of Ca in column effluent were highest in the bottom column but this did not coincide with higher concentrations of Al.

At this time the elements of concern are not being released from the bottom column. As mentioned previously, the high concentration of Ca could be a risk to local benthic communities (Piatak et al. 2019).

3.4 References

Cotten, J., Le Dez, A., Bau, M., Caroff, M., Maury, R. C., Dulski, P., and Brousse, R. 1995. Origin of anomalous rare-earth element and yttrium enrichments in subaerially exposed basalts: evidence from French Polynesia. *Chemical Geology*, *119*(1-4), 115-138.

De Windt, L., Chaurand, P., and Rose, J. 2011. "Kinetics of steel slag leaching: batch tests and modeling." *Waste management*. 2(31): 225-235.

Glasser, F. P. 1992. Progress in the immobilization of radioactive wastes in cement. *Cement and concrete research*, *22*(2-3), 201-216.

Hobson, A. J., Stewart, D. I., Mortimer, R. J., Mayes, W. M., Rogerson, M., & Burke, I. T. (2018). Leaching behaviour of co-disposed steel making wastes: Effects of aeration on leachate chemistry and vanadium mobilisation. *Waste management*, *81*, 1-10.

Hudson-Edwards, K. A., Schell, C., and Macklin, M. G. 1999. Mineralogy and geochemistry of alluvium contaminated by metal mining in the Rio Tinto area, southwest Spain. *Applied Geochemistry*, *14*(8), 1015-1030.

Meima, J. A., and Comans, R. N. 1999. The leaching of trace elements from municipal solid waste incinerator bottom ash at different stages of weathering. *Applied Geochemistry*, *14*(2), 159-171.

Mitchell, R. H., and Mariano, A. N. 2016. Primary phases in aluminous slags produced by the aluminothermic reduction of pyrochlore. *Mineralogical Magazine*, *80*(2), 383-397.

Monnin, C., and Cividini, D. 2006. The saturation state of the world's ocean with respect to (Ba, Sr) SO4 solid solutions. *Geochimica et Cosmochimica Acta*, *70*(13), 3290-3298.

Parkhurst DL, and Appelo CAJ .2013. "Description of input and examples for PHREEQC version 3–A computer program for speciation, batch-reaction, one-dimensional transport, and inverse geochemical calculations" Techniques and Methods (6).

Petrunic, B. M., and Al, T. A. 2005. Mineral/water interactions in tailings from a tungsten mine, Mount Pleasant, New Brunswick. *Geochimica et Cosmochimica Acta*, *69*(10), 2469-2483.

Piatak, N. M., Parsons, M. B., and Seal II, R. R. 2015. Characteristics and environmental aspects of slag: A review. *Applied Geochemistry*, *57*, 236-266.

Piatak, N. M., Seal, R. R., Hoppe, D. A., Green, C. J., and Buszka, P. M. 2019. Geochemical Characterization of Iron and Steel Slag and Its Potential to Remove Phosphate and Neutralize Acid. *Minerals*, *9*(8), 468.

Tossavainen, Mia. Leaching results in the assessement of slag and rock materials as construction material. PhD. Diss. Luleå tekniska universitet, 2005.

Warchulski, R., Gawęda, A., Kądziołka-Gaweł, M., and Szopa, K. 2015. Composition and element mobilization in pyrometallurgical slags from the Orzeł Biały smelting plant in the Bytom–Piekary Śląskie area, Poland. *Mineralogical Magazine*, *79*(2), 459-483.

4 Conclusions

This study successfully characterized the weathering and leaching properties of slag from Oka, Quebec. The data collected from the column leaching experiment is characterized by high pH and high alkalinity. Overall, high concentrations of Al, Na, and K in effluent are likely a result of dissolution of aluminate and lower abundance aluminosilicate minerals. High concentrations of Al Ca, Na, K, and F in the top column leachate are likely a result of intersistial aluminate glass and anorthite glass weathering. This assumption coincides with analyses of secondary minerals where Al- and/or Ca- hydroxide coatings as weathering products were identified. The middle column also had elevated Al, Ca, Na, and K concentrations in the effluent likely a result of aluminosilicate glass dissolution. In general, the lower concentrations reported in the bottom column are a result of preferential dissolution of ferri-gehlenite forming Fe-oxyhydroxides then Al and Si precipitates.

It is evident that the study of nanoscale environments is important to further the understanding of weathering and leaching environments in mine waste systems. This is demonstrated by the detection of nanoscale variations in secondary materials. Albeit, large scale mineralogical investigations provide important estimates of weathering environments, nanoscale analyses provide a more detailed understanding of weathering reactions.

Appendix A: Lithogeochemistry

A.1 Methods

Samples from representing the top, middle and bottom of the slag were analyzed for lithogeochemistry. Crushed samples were submitted to Actlabs for the samples to be analyzed using the “4B2-Lithium Metaborate/Tetraborate Fusion – ICP/MS” package. Samples fused under 4B2 are diluted and analyzed by Perkin Elmer Sciex Elan 6000, 6100 or 9000 ICP/MS. Three blanks and five controls are analyzed per group of samples. Duplicates are fused and analyzed every 15 samples. Instrument is recalibrated every 40 sample. Table 3-5 contain oxide and elemental data and Table 6-8 contain certified reference material data.

Table 3. Lithogeochemistry results (Part 1)

Analyte Symbol	SiO2	Al2O3	Fe2O3(T)	MnO	MgO	CaO	Na2O	K2O	TiO2	P2O5	Sc	Be	V	Ba	Sr	Y	Zr	Cr	Co	Ni	Cu	Zn
Unit Symbol	%	%	%	%	%	%	%	%	%	%	ppm	ppm	ppm	ppm	ppm	ppm	ppm	ppm	ppm	ppm	ppm	ppm
Detection Limit	0.01	0.01	0.01	0.001	0.01	0.01	0.01	0.01	0.001	0.01	1	1	5	2	2	1	2	20	1	20	10	30
Analysis Method	FUS-ICP	FUS-ICP	FUS-ICP	FUS-ICP	FUS-ICP	FUS-ICP	FUS-ICP	FUS-ICP	FUS-ICP	FUS-ICP	FUS-ICP	FUS-ICP	FUS-ICP	FUS-ICP	FUS-ICP	FUS-ICP	FUS-ICP	FUS-MS	FUS-MS	FUS-MS	FUS-MS	FUS-MS
COL 001	1.12	46.08	0.09	0.201	1.38	16.38	0.49	0.04	5.323	0.02	21	2	24	1468	3596	779	9803	370	< 1	30	< 10	< 30
COL 002	3.38	47.52	0.07	0.125	0.61	17.79	3.44	0.11	5.788	< 0.01	28	2	24	1799	5434	895	> 10000	50	< 1	< 20	< 10	< 30
COL 003	15.33	49.8	6.75	0.372	0.41	24.65	0.1	0.09	0.202	0.02	6	4	43	128	191	198	197	980	6	450	50	< 30
MIN 001	2.09	46.71	0.09	0.221	1.52	17.01	0.48	0.03	5.64	0.02	22	2	26	1653	3854	839	> 10000	360	2	< 20	40	< 30
MIN 002	71.68	11.87	0.91	0.054	0.17	6.32	1.08	0.11	1.523	0.06	7	< 1	19	805	1406	225	3188	610	5	330	10	< 30
MIN 003	76.35	9.12	1.16	0.057	0.19	5.03	0.7	0.07	1.118	< 0.01	6	< 1	18	615	1118	232	3018	1070	7	610	30	< 30
MIN 004	3.51	60.3	6.22	0.258	1.28	10.45	1.57	0.09	3.49	< 0.01	22	2	80	967	3268	416	4375	940	4	480	50	< 30
MIN 005	15.23	51.75	5.19	0.336	0.37	24.96	0.06	0.08	0.149	0.03	5	4	39	120	158	188	298	480	3	200	50	< 30
MIN 006	0.51	45.44	0.32	0.077	0.23	16.73	0.5	0.21	6.042	0.02	29	2	25	693	3544	880	> 10000	260	2	140	< 10	< 30
MIN 007	0.85	47.06	0.02	0.25	1.41	17.46	1.86	0.21	7.076	< 0.01	22	2	41	2639	4150	709	> 10000	30	2	< 20	< 10	< 30
MIN 008	75.6	9.34	1.15	0.053	0.19	5	0.65	0.07	1.109	< 0.01	5	< 1	19	594	1076	210	2696	1030	7	580	20	< 30

Table 4. Lithogeochemistry results (Part 2)

Analyte Symbol	Ga	Ge	As	Rb	Nb	Mo	Ag	In	Sn	Sb	Cs	La	Ce	Pr	Nd
Unit Symbol	ppm	ppm	ppm	ppm	ppm	ppm	ppm	ppm	ppm	ppm	ppm	ppm	ppm	ppm	ppm
Detection Limit	1	1	5	2	1	2	0.5	0.2	1	0.5	0.5	0.1	0.1	0.05	0.1
Analysis Method	FUS-MS	FUS-MS	FUS-MS	FUS-MS	FUS-MS	FUS-MS	FUS-MS	FUS-MS	FUS-MS	FUS-MS	FUS-MS	FUS-MS	FUS-MS	FUS-MS	FUS-MS
COL 001	82	7	28	< 2	> 1000	3		< 0.2	< 1	< 0.5	< 0.5	> 2000	> 3000	> 1000	> 2000
COL 002	76	6	20	< 2	> 1000	< 2		< 0.2	< 1	< 0.5	< 0.5	> 2000	> 3000	> 1000	> 2000
COL 003	14	< 1	< 5	5	922	46	1.4	< 0.2	1	< 0.5	0.7	267	1330	86	280
MIN 001	81	8	26	< 2	> 1000	3		< 0.2	7	< 0.5	< 0.5	> 2000	> 3000	> 1000	> 2000
MIN 002	20	2	7	3	> 1000	24		< 0.2	< 1	< 0.5	< 0.5	1520	> 3000	630	1920
MIN 003	12	1	< 5	2	> 1000	44		< 0.2	< 1	< 0.5	< 0.5	1140	> 3000	506	1550
MIN 004	72	5	17	< 2	> 1000	26		< 0.2	6	< 0.5	< 0.5	> 2000	> 3000	> 1000	> 2000
MIN 005	14	< 1	< 5	5	272	17	1.4	< 0.2	3	< 0.5	0.6	165	678	52.7	188
MIN 006	104	10	35	< 2	> 1000	11		< 0.2	< 1	< 0.5	< 0.5	> 2000	> 3000	> 1000	> 2000
MIN 007	71	8	29	4	> 1000	< 2		< 0.2	< 1	< 0.5	< 0.5	> 2000	> 3000	> 1000	> 2000

Table 5. Lithogeochemistry results (Part 3)

Analyte Symbol	Sm	Eu	Gd	Tb	Dy	Ho	Er	Tm	Yb	Lu	Hf	Ta	W	Tl	Pb	Bi	Th	U
Unit Symbol	ppm	ppm	ppm	ppm	ppm	ppm	ppm	ppm	ppm	ppm	ppm	ppm	ppm	ppm	ppm	ppm	ppm	ppm
Detection Limit	0.1	0.05	0.1	0.1	0.1	0.1	0.1	0.05	0.1	0.01	0.2	0.1	1	0.1	5	0.4	0.1	0.1
Analysis Method	FUS-MS	FUS-MS	FUS-MS	FUS-MS	FUS-MS	FUS-MS	FUS-MS	FUS-MS	FUS-MS	FUS-MS	FUS-MS	FUS-MS	FUS-MS	FUS-MS	FUS-MS	FUS-MS	FUS-MS	FUS-MS
COL 001	> 1000	275	364	53.8	274	40	94.8	11.5	63	6.83	29.3	> 500	< 1	0.4	6	< 0.4	1660	778
COL 002	> 1000	273	383	57	284	41	94.3	11.2	61.4	7.25	48.5	> 500	2	0.5	< 5	< 0.4	> 2000	> 1000
COL 003	47.9	21.2	32.1	5.5	35.9	6.8	20.5	3.13	20	2.92	8.3	16.2	> 5000	0.3	< 5	< 0.4	43.3	25
MIN 001	986	289	370	56.2	288	45.1	103	13	68.1	7.43	32	> 500	137	0.2	6	< 0.4	1580	790
MIN 002	273	65.3	108	15.4	79.9	12.7	27.5	3.29	17.4	2.02	16.2	95.7	168	0.2	< 5	< 0.4	1210	324
MIN 003	238	61.2	101	15.3	75.4	11	24.9	3	16.5	1.95	11.2	175	10	0.4	< 5	< 0.4	698	291
MIN 004	671	195	213	30.2	144	19.3	43.7	4.84	27	3.35	18.5	> 500	4	0.4	< 5	< 0.4	1250	424
MIN 005	37.2	18.2	29.7	5.2	34.7	6.6	20.1	3.1	20.3	2.73	8.9	6.4	> 5000	0.1	< 5	< 0.4	27.5	17.4
MIN 006	> 1000	337	462	65.9	328	49.1	111	14.4	72.6	7.97	42.8	> 500	145	< 0.1	< 5	< 0.4	> 2000	> 1000
MIN 007	991	241	373	52.2	253	37.3	82.9	10	52.3	5.85	40.2	> 500	43	< 0.1	< 5	< 0.4	> 2000	> 1000

Table 6. Lithogeochemistry QC results (Part 1)

Analyte Symbol	SiO2	Al2O3	Fe2O3(T)	MnO	MgO	CaO	Na2O	K2O	TiO2	P2O5	Sc	Be	Ba	Sr	Y	Zr	Cr	Co	Ni	Cu	Zn
Unit Symbol	%	%	%	%	%	%	%	%	%	%	ppm	ppm	ppm	ppm	ppm	ppm	ppm	ppm	ppm	ppm	ppm
Detection Limit	0.01	0.01	0.01	0	0.01	0	0.01	0	0	0	1	1	2	2	1	2	20	1	20	10	30
NIST 694 Meas	11.7	1.84	0.72	0.01	0.34	43	0.87	0.5	0.1	42											
NIST 694 Cert	11.2	1.8	0.79	0.01	0.33	44	0.86	0.5	0.1	30											
NIST 694 Meas	11.4	1.9	0.75	0.01	0.33	42	0.86	0.5	0.1	30											
NIST 694 Cert	11.2	1.8	0.79	0.01	0.33	44	0.86	0.5	0.1	30											
DNC-1 Meas	47.5	19.3	10.13	0.15	10.1	12	1.97	0.2	0.5	0	32		108	153	16	36	280	62	260	110	80
DNC-1 Cert	47.15	18.34	9.97	0.150	10.13	11.49	1.890	0.234	0.480	0.070	31		118	144.0	18.0	38	270	57	247	100	70
LKSD-3 Meas																	90	32	50	40	140
LKSD-3 Cert																	87	30	47	35	152
TDB-1 Meas																	240		90	330	150
TDB-1 Cert																	251		92	323	155
W-2a Meas	52.2	15.2	10.65	0.16	6.1	11	2.23	0.6	1.1	0	35	< 1	174	198	19	90	100	45	80	110	80
W-2a Cert	52.4	15.4	10.7	0.16	6.37	11	2.14	0.6	1.1	0	36	1	182	190	24	94	92	43	70	110	80
SY-4 Meas	50.1	20.8	6.21	0.11	0.52	8.2	6.95	1.7	0.3	0	< 1	3	347		119	522					
SY-4 Cert	49.9	20.69	6.21	0.108	0.54	8.05	7.10	1.66	0.287	0.131	1.1	2.6	340		119	517					
CTA-AC-1 Meas																				60	
CTA-AC-1 Cert																				54.0	
BIR-1a Meas	48	16.1	11.33	0.17	9.39	14	1.82	0	1	0	43	< 1	7	113	14	15	390	56	180	130	70
BIR-1a Cert	47.96	15.50	11.30	0.175	9.700	13.30	1.82	0.030	0.96	0.021	44	0.58	6	110	16	18	370	52	170	125	70
NCS DC86312 Meas																					
NCS DC86312 Cert																					
NCS DC70009 (GBW07241) Meas																		3		###	90
NCS DC70009 (GBW07241) Cert																		3.7		960	100
OREAS 100a (Fusion) Meas																		18		180	
OREAS 100a (Fusion) Cert																		18.1		169	
OREAS 101a (Fusion) Meas																		51		450	
OREAS 101a (Fusion) Cert																		48.8		430	
OREAS 101b (Fusion) Meas																		45	< 20	420	
OREAS 101b (Fusion) Cert																		47	9	420	
JR-1 Meas																		1	< 20	< 10	
JR-1 Cert																		0.83	1.67	2.68	
Method Blank	0.01	< 0.01	< 0.01	0	0.01	< 0.01	< 0.01	< 0.01	< 0.001	< 0.01	< 1	< 1	< 2	< 2	< 1	< 2					
Method Blank	0.01	< 0.01	< 0.01	0	0.01	< 0.01	< 0.01	< 0.01	< 0.001	< 0.01	< 1	< 1	< 2	< 2	< 1	2	< 20	< 1	< 20	< 10	< 30

Certified reference material ID is in the left column, "-cert" are certified reference material expected values and "-meas" is the measured value.

Table 7. Lithogeochemistry QC results (Part 2)

Report Date: 15/6/2018																						
Analyte Symbol	Ga	Ge	As	Rb	Nb	Mo	Ag	In	Sn	Sb	Cs	La	Ce	Pr	Nd	Sm	Eu	Gd	Tb	Dy	Ho	Er
Unit Symbol	ppm	ppm	ppm	ppm	ppm	ppm	ppm	ppm	ppm	ppm	ppm	ppm	ppm	ppm	ppm	ppm	ppm	ppm	ppm	ppm	ppm	ppm
Detection Limit	1	1	5	2	1	2	0.5	0.2	1	0.5	0.5	0.1	0.1	0.05	0.1	0.1	0.05	0.1	0.1	0.1	0.1	0.1
NIST 694 Meas																						
NIST 694 Cert																						
NIST 694 Meas																						
NIST 694 Cert																						
DNC-1 Meas	14			5						1		3.7			5		0.62					
DNC-1 Cert	15			5						0.96		3.6			5.20		0.59					
LKSD-3 Meas			26	71		< 2	2.8		2		2.4	48	89.2		44.6	7.9	1.5		0.9	5.1		
LKSD-3 Cert			27	78		2	2.7		3		2.3	52	90		44	8	1.5		1	4.9		
TDB-1 Meas												18	44.5		25.3		2.1			7.6		
TDB-1 Cert												17	41		23		2.1			8		
W-2a Meas	19	2		20	7	< 2					0.8	10.5	25.1		13.7	3.5	1.1		0.7	3.8	0.8	2.3
W-2a Cert	17	1		21	7.9	0.6					0.99	10	23		13	3.3	1		0.63	3.6	0.76	2.5
SY-4 Meas																						
SY-4 Cert																						
CTA-AC-1 Meas												> 2000	> 3000		1140	165	46.1	131	14.4			
CTA-AC-1 Cert												2176	3326		1087	162	46.7	124	13.9			
BIR-1a Meas	16											0.6	1.9		2.5	1.1	0.52	1.9		3.8		
BIR-1a Cert	16											0.63	1.9		2.5	1.1	0.55	2.0		4		
NCS DC86312 Meas												> 2000	174		1550			231	31.2	190	35.2	101
NCS DC86312 Cert												2360	190		1600			225.0	34.6	183	36	96.2
NCS DC70009 (GBW07241) Meas	16	11	64	503			1.9	1		2.9	43.8	24	61.4	8.2	33.5	12.5	0.16	15.4	3.1	22.1	4.3	13.9
NCS DC70009 (GBW07241) Cert	16.5	11.2	69.9	500			1.8	1.3		3.1	41	23.7	60.3	7.9	32.9	12.5	0.16	14.8	3.3	20.7	4.5	13.4
OREAS 100a (Fusion) Meas						23						260	468	46.4	149	23.3	3.67	22.8	3.8	23.6	4.8	15
OREAS 100a (Fusion) Cert						24.1						260	463	47.1	152	23.6	3.71	23.6	3.80	23.2	4.81	14.9
OREAS 101a (Fusion) Meas						21						803	1380	128	389	48.7	8.04	44.9	5.7	33	6.3	19.8
OREAS 101a (Fusion) Cert						21.9						816	1396	134	403	48.8	8.06	43.4	5.92	33.3	6.46	19.5
OREAS 101b (Fusion) Meas						20						811	1410	131	390	50	8.32		5.3	32.3	6.4	19
OREAS 101b (Fusion) Cert						21						789	1331	127	378	48	7.77		5.37	32.1	6.34	18.7
JR-1 Meas	17	2	16	243	15	3		< 0.2	3		20.7	20.2	47.6	6.1	23.7	5.7	0.28		1	5.5	1.1	
JR-1 Cert	16.1	1.88	16.3	257	15.2	3.25		0.028	2.86		20.8	19.7	47.2	5.58	23.3	6.03	0.30		1.01	5.69	1.11	
Method Blank							<							<			<					
Method Blank	< 1	< 1	< 5	< 2	< 1	< 2	0.5	< 0.2	< 1	< 0.5	< 0.5	< 0.1	< 0.1	0.05	< 0.1	< 0.1	0.05	< 0.1	< 0.1	< 0.1	< 0.1	< 0.1

Certified reference material ID is in the left column, “-cert” are certified reference material expected values and “-meas” is the measured value.

Table 8. Lithogeochemistry QC results (Part 3)

Analyte Symbol	Tm	Yb	Lu	Hf	Ta	W	Tl	Pb	Bi	Th	U
Unit Symbol	ppm	ppm	ppm	ppm	ppm	ppm	ppm	ppm	ppm	ppm	ppm
Detection Limit	0.05	0.1	0.01	0.2	0.1	1	0.1	5	0.4	0.1	0.1
NIST 694 Meas											
NIST 694 Cert											
NIST 694 Meas											
NIST 694 Cert											
DNC-1 Meas		2.1						6			
DNC-1 Cert		2.0						6.3			
LKSD-3 Meas		2.7	0.42	4.5						11.4	4.7
LKSD-3 Cert		2.7	0.4	4.8						11.4	4.6
TDB-1 Meas		3.2								2.9	
TDB-1 Cert		3.4								2.7	
W-2a Meas		2.1	0.33	2.6	0.5	< 1	0.6	10	< 0.4	2.4	0.5
W-2a Cert		2.1	0.33	2.6	0.5	0.3	0.2	9.3	0.03	2.4	0.53
SY-4 Meas											
SY-4 Cert											
CTA-AC-1 Meas		11.3			2.8						4.5
CTA-AC-1 Cert		11.4			2.65						4.4
BIR-1a Meas		1.7		0.6				< 5			
BIR-1a Cert		1.7		0.60				3			
NCS DC86312 Meas	13.8	88.5	12.6								
NCS DC86312 Cert	15.1	87.79	11.96								
NCS DC70009 (GBW07241) Meas	2.3	16.1	2.33			2300	1.9			30.9	
NCS DC70009 (GBW07241) Cert	2.2	14.9	2.4			2200	1.8			28.3	
OREAS 100a (Fusion) Meas	2.32	15.7	2.29							54.3	139
OREAS 100a (Fusion) Cert	2.31	14.9	2.26							51.6	135
OREAS 101a (Fusion) Meas	2.8	18.3	2.63							37.2	452
OREAS 101a (Fusion) Cert	2.90	17.5	2.66							36.6	422
OREAS 101b (Fusion) Meas	2.75	17.9	2.58							37.4	404
OREAS 101b (Fusion) Cert	2.66	17.6	2.58							37.1	396
JR-1 Meas	0.67	4.7	0.67	4.1			1.5	20	0.5	28.9	8.9
JR-1 Cert	0.67	4.55	0.71	4.51			1.56	19.3	0.56	26.7	8.88
Method Blank											
Method Blank	< 0.05	< 0.1	< 0.01	< 0.2	< 0.1	< 1	< 0.1	< 5	< 0.4	< 0.1	< 0.1

Certified reference material ID is in the left column, "-cert" are certified reference material expected values and "-meas" is the measured value.

Appendix B: Autoradiography

B.1 Methods

Autoradiography is used in order to detect and map radioactive minerals in samples. The methods used to assess radioactivity in the slag adheres to the method followed by Percival et al. 2006 whereby polished thin sections were placed right side up under thin strips of Agfa Structurix D8 FW industrial X-ray film and set in dark boxes for a 6-week period. After 6 weeks each box was opened and the X-ray films were developed After developing, the negatives were scanned and saved as .tiff files. Images were correlated with mineral distributions in the thin sections in order to identify the most radioactive phases.

B.2 Results

Visually radiation does not appear to be concentrated within secondary material. In the top and middle samples there's no radioactivity in the secondary phases as well as hibonite rich areas are concentrated in the matrix (Fig. 21. The radioactivity is concentrated in the calcium zirconate phases which are enclosed in perovskite with relatively less radioactivity in the perovskite. Radiation is noted in the mineralogical samples from the top and middle of slag pit which has significant perovskite and calcium zirconate phases (Fig 21). There are two major types of perovskites found in the top samples, the perovskites with higher Al, Ti, Ca and REE contents and with enclosed calcium zirconate exhibit more radiation (Fig. 21). Samples from the bottom did not exhibit any radioactivity.

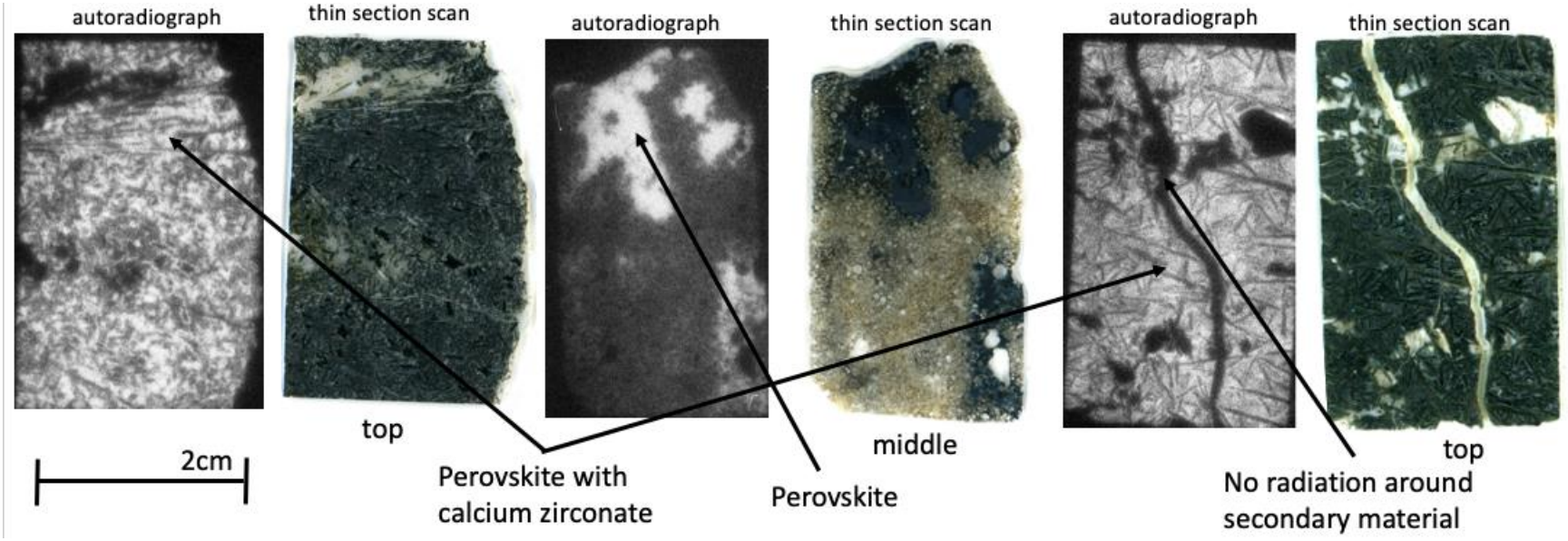

Figure 21. Autoradiography results showing distribution of radiological minerals of the slag in comparison to the scanned thin section of the same sample. Autoradiograph on left. Location where slag cooled in the slag pit is noted below the thin section scan image.

4.1 References

Dudek, M., and Rapacz-Kmita, A. 2013. CaZrO 3-based powders suitable for manufacturing electrochemical oxygen probes. *Central European Journal of Chemistry*, *11*(12), 2088-2097.

Percival, J.B., Potter, E.G., Lauzière, K., Ijewliw, O., Bilot, I., Hunt, P., English, M.L.R., Olejarz, A.D., Laudadio, A.B., Enright, A., Robillard, K.-L. and Corriveau, L. 2015. Mineralogy, petrography and autoradiography of selected samples from the Contact Lake and NICO Areas, Great Bear Magmatic Zone, Northwest Territories (IOCG-GEM Project). Geological Survey of Canada Open File 7755

Appendix C: Aqueous Geochemistry

C.1 Methods

A more detailed description of sampling methods used to collect slag for aqueous geochemical analysis is provided in Chapter 2. In general, samples were obtained from crushed and sieved slag representative of the top, middle, and bottom sections of the slag. Columns were packed with slag and injected with a simulated precipitation. The leachate was analyzed by inductively coupled plasma optical emission spectroscopy (ICP-OES), anion chromatography (IC) and inductively coupled plasma mass spectroscopy (ICP-MS).

ICP-OES, IC, and ICP-MS analyses were conducted at the University of Ottawa in the geochemistry lab. ICP-OES values were obtained for trace elements and major cations as well as total sulfur (TS). The second set of analyses were obtained by IC involved analysis for anions including Cl, F, NO_3, SO_4, PO_4. Certified reference material was used to assess accuracy and precision. ICP-MS was used to obtain values for trace elements and major cations, however, data was low quality in terms of precision, accuracy and charge balance, therefore, ICP-OES was used. Results from ICP-MS are in Table 16-18 and Figure 19 shows a comparison between results from ICP-OES and ICP-MS for select elements. ICP-OES and ICP-MS runs included a high concentration groundwater standard, a low concentration groundwater standard, and a seawater standard were used as certified reference material. Table 9-11 contains cation data and Table 12 has the RSD and RE for the ICP-OES data. Table 13-15 contain anion data. Methods for determining RSD values can be found in Appendix D.

ICP-OES samples were analyzed with a dilution factor ranging from 5 to 2000 using trace-metal grade nitric acid solution (0.2 N). A sample of the 0.2 N solution was analyzed by

ICP-OES to provide an estimate of contamination by acidification. In all cases the contamination was incredibly minor (Table 12) however, the blank values were not subtracted from the diluted samples prior to the dilution factors application to the dataset. As a result, contamination can be magnified anywhere from 5 to 2000 fold.

Table 9. ICP-OES geochemistry results (top column)

	Day	Al	Ba	Ca	Fe	K	Li	Mg	Mn	Na	S	Sr
C2 S3 x2000	42	3025.14	0.90	21.00	3.27	341.91	7.43	1.40	0.16	14984.48	131.76	0.16
C2 S4 x1250	56	997.36	0.62	11.73	2.11	50.73	5.60	1.20	0.12	3075.66	50.43	2.01
C2 S5 x1000	70	1705.10	0.54	12.18	0.92	174.48	3.77	0.86	0.07	7775.17	68.29	0.86
C2 S6 x500	82	516.00	0.93	8.11	0.29	22.83	2.94	0.21	0.03	1550.42	14.12	3.92
C2 S7 x500	94	1866.97	0.17	2.33	0.33	141.32	2.30	0.23	0.05	7813.32	38.22	0.31
C2 S8 x1000	108		0.25	209.73	1.07	6.41	9.13	0.87	0.07		36.60	0.23
C2 S9 x500	122	396.31	2.31	15.08	0.76	17.72	4.12	0.17	0.05	1272.07	17.00	8.89
C2 S10 x500	134	273.54	7.81	28.19	0.49	13.72	4.97	0.24	0.03	964.93	14.30	25.30
C2 S11 x500	146	152.02	12.38	41.25	0.50	14.18	7.34	0.63	0.06	708.17	16.42	42.94
C2 S12 x500	158	124.56	13.28	50.27	0.52	11.50	6.21	0.46	0.04	582.21	16.40	51.70
C2 S13 x500	168	153.19	15.71	41.17	0.48	10.37	8.15	0.44	0.04	556.37	15.09	52.63
C2 S14 x500	180	128.90	22.23	51.88	0.49	13.67	8.25	0.32	0.03	629.32	17.46	69.71
C2 S15 x1000	192	180.65	39.45	87.56	1.23	9.19	17.12	0.95	0.09	467.11	28.56	103.48
C2 S16 x1000	204	125.32	38.11	102.93	1.86	16.61	13.33	1.69	0.10	467.69	31.62	101.01
C2 S18 x1000	216	92.25	33.93	79.14	1.60	9.02	12.92	1.01	0.10	367.12	30.60	89.32
C2 S19 x1000	228	84.70	27.33	64.15	1.06	5.39	13.86	0.95	0.10	362.71	29.02	66.21
C2 S20 x1000	238	77.40	42.14	103.22	0.88	6.58	15.28	0.74	0.08	313.53	25.67	101.00
C2 S21 x1000	250	73.03	33.99	89.72	0.90	5.64	15.60	1.00	0.09	285.32	37.39	78.19
C2 S23 x1000	262	49.02	0.95	9.91	0.97	6.86	14.98	0.90	0.08	292.62	33.61	7.28
C2 S24 x500	272	69.52	14.57	21.38	0.51	8.90	14.90	0.52	0.05	237.25	15.70	39.60
C2 S25 x1000	284		33.60	96.14	3.39	9.63	16.37	0.93	0.08	248.99	25.17	66.98
C2 S3 x2000	42	3025.14	0.90	21.00	3.27	341.91	7.43	1.40	0.16	14984.48	131.76	0.16
C2 S4 x1250	56	997.36	0.62	11.73	2.11	50.73	5.60	1.20	0.12	3075.66	50.43	2.01
C2 S5 x1000	70	1705.10	0.54	12.18	0.92	174.48	3.77	0.86	0.07	7775.17	68.29	0.86
C2 S6 x500	82	516.00	0.93	8.11	0.29	22.83	2.94	0.21	0.03	1550.42	14.12	3.92
C2 S3 x50	42	3168.91	0.33	4.83	0.06	538.57	0.60	0.06	0.00		67.35	0.41
C2 S4 x50	56	1075.68	0.40	4.01	0.04	82.82	1.17	0.05	0.00		3.70	2.34
C2 S5 x50	70	1785.49	0.22	5.62	0.05		0.89	0.05	0.00		42.88	1.31
C2 S6 x10	82	622.91	0.89	8.03	0.01	54.10	2.08	0.01	0.00		1.09	5.51
C2 S7 x25	94	3036.51	0.10	1.79	0.02		0.73	0.02	0.00		31.55	0.60
C2 S8 x50	108	17.42	0.17		0.09	12.58	5.08	0.14	0.01	21.66	2.91	0.43
C2 S9 x25	122	409.55	2.09	13.95	0.02	36.16	2.50	0.03	0.00	1186.38	1.24	10.11
C2 S10 x25	134	265.49	7.16	25.46	0.03	27.65	3.58	0.03	0.00	872.05	0.87	28.56
C2 S11 x25	146	163.45	12.17	37.29	0.03	21.35	6.01	0.03	0.00	660.32	0.96	51.10
C2 S12 x25	158	123.87	12.33	43.30	0.04	17.00	4.32	0.08	0.00	489.56	2.42	55.42
C2 S13 x25	168	158.56	15.30	38.05	0.03	16.69	6.72	0.03	0.00	499.81	0.95	60.45
C2 S14 x25	180	135.83	21.91	49.20	0.03	20.65	7.26	0.04	0.00	585.87	1.45	82.20
C2 S15 x50	192	177.14	38.83	79.84	0.09	15.13	13.83	0.06	0.00	413.49	1.85	112.23
C2 S16 x50	204	123.15	37.27	93.76	0.15	22.94	9.45		0.01	401.93	2.37	108.43
C2 S18 x50	216	88.35	32.91	69.92	0.06	12.61	9.09	0.05	0.00	308.51	1.39	94.57
C2 S19 x50	228	81.73	26.86	56.01	0.08	12.28	9.92	0.05	0.00	305.57	1.46	71.16
C2 S20 x50	238	72.83	41.13	93.83	0.07	10.97	11.14	0.05	0.00	256.41	1.67	106.04
C2 S21 x50	250	68.70	33.28	80.71	0.06	9.96	11.29	0.05	0.01	223.74	1.58	82.11
C2 S23 x50	262	44.84			0.09	11.60	10.44	0.05	0.00	213.59	1.58	
C2 S24 x50	272	64.78	13.46		0.08	13.76	12.01	0.05	0.01	202.18	1.33	39.15
C2 S25 x50	284	531.09	33.35	87.74		13.58	12.79	0.04	0.01	193.85	1.20	71.74
C2 S3 x50	42	3168.91	0.33	4.83	0.06	538.57	0.60	0.06	0.00		67.35	0.41
C2 S4 x50	56	1075.68	0.40	4.01	0.04	82.82	1.17	0.05	0.00		3.70	2.34
C2 S5 x50	70	1785.49	0.22	5.62	0.05		0.89	0.05	0.00		42.88	1.31
C2 S6 x10	82	622.91	0.89	8.03	0.01	54.10	2.08	0.01	0.00		1.09	5.51
C2 S7 x25	94	3036.51	0.10	1.79	0.02		0.73	0.02	0.00		31.55	0.60
C2 S8 x50	108	17.42	0.17		0.09	12.58	5.08	0.14	0.01	21.66	2.91	0.43
C2 S9 x25	122	409.55	2.09	13.95	0.02	36.16	2.50	0.03	0.00	1186.38	1.24	10.11

Blank values were outlier not used for plots, red values were over calibration curve and green values were the samples used for plotting.

Table 10. ICP-OES geochemistry results (middle column)

Blank values were outlier not used for plots, red values were over calibration curve and green values were the samples used for plotting.

Sample Code	Day	Al	Ba	Ca	Fe	K	Li	Mg	Mn	Na	S	Sr
C1 S1 x250	16	74.25	19.93	245.36	0.18	81.41	1.75	0.28	0.03	1351.28	9.29	89.28
C1 S2 x250	30	102.59	21.97	306.22	0.21	104.02	1.76	0.15	0.02	1697.29	8.65	96.59
C1 S3 x250	42	126.73	17.01	168.52	0.27	82.66	1.63	0.14	0.02	1415.31	10.63	71.91
C1 S4 x250	52	223.30	20.50	204.25	0.27	69.31	1.73	0.15	0.02	1202.57	10.44	88.75
C1 S5 x250	62	220.86	0.14		0.23	14.43	7.62	0.16	0.02		7.91	
C1 S6 x250	72		7.44	77.26	0.23		1.70	0.13	0.02		44.52	34.05
C1 S7 x250	82	142.64	11.30	117.04	0.21	30.90	1.63	0.08	0.03	588.45	7.66	49.03
C1 S8 x100	92	148.77	11.89	133.34	0.08	25.59	1.24	0.05	0.01	421.03	4.31	50.91
C1 S9 x100	102	163.83	13.82	171.61	0.09	21.58	1.36	0.06	0.01	354.68	4.01	56.75
C1 S10 x100	112	77.39	11.54	147.50	0.09	18.09	1.33	0.05	0.01	298.44	3.39	45.73
C1 S11 x100	122	120.67	11.74	174.01	0.07	16.34	1.41	0.06	0.01	261.45	3.76	44.90
C1 S12 x100	132	84.08	10.92	182.40	0.13	10.89	1.29	1.16	0.01	186.37	5.04	39.14
C1 S13 x100	142	110.13	9.23	159.75	0.08	12.29	1.36	0.06	0.01	195.50	3.72	34.82
C1 S14 x100	152	85.37	10.98	166.26	0.10	11.87	1.40	0.06	0.01	188.50	3.44	39.99
C1 S15 x100	162	72.43	9.76	170.09	0.09	9.98	1.43	0.04	0.01	154.01	2.97	34.26
C1 S16 x100	172	38.63	10.01	167.41	0.10	9.38	1.50	0.06	0.01	149.95	2.97	34.85
C1 S17 x100	182	71.91	11.95	206.01	0.08	9.91	1.49	0.05	0.01	149.42	3.95	41.03
C1 S18 x100	192	94.19	10.91	222.39	0.12	9.75	1.46	0.07	0.01	149.62	4.54	36.98
C1 S19 x100	202	96.84	7.27	161.28	0.11	8.15	1.44	0.06	0.01	128.88	2.75	25.25
C1 S20 x100	212	145.53	9.75	192.90	0.10	10.18	1.51	0.13	0.01	180.57	5.47	31.93
C1 S21 x100	222											
C1 S22 x100	232	52.80	8.58	127.50	0.10	7.47	1.48	0.06	0.01	122.56	3.45	28.94
C1 S23 x100	242	87.24	11.88	205.44	0.14	8.76	1.63	0.15	0.01	126.64	4.55	38.75
C1 S24 x100	252	64.07	9.66	195.35	0.07	8.17	1.53	0.04	0.01	104.45	3.26	31.33
C1 S25 x100	262	61.77	6.86	122.94	0.08	5.88	1.48	0.05	0.01	100.27	3.24	21.53
C1 S26 x100	272	76.54	8.34	171.87	0.45	5.85	1.59	0.08	0.01	98.58	3.84	27.60
C1 S27 x100	282		2.97		0.49	5.66	1.52	0.06	0.01	111.75	3.87	
C1 S1 x10	16	100.50	23.01	294.67	0.067	139.26	1.60	0.26	0.0039	#VALUE!	2.59	148.26
C1 S2 x10	30	115.54	19.77	284.09	0.096	139.14	1.14	0.03	0.0025	#VALUE!	1.30	125.83
C1 S3 x10	42	133.15	15.55	166.81	0.018	113.38	0.87	0.01	0.0010	#VALUE!	1.16	93.14
C1 S4 x10	52	259.72	18.97	196.22	0.021	100.03	1.09	0.01	0.0007	#VALUE!	1.07	113.27
C1 S5 x10	62	231.13		418.27	0.018	22.64	7.69	0.03	0.0015	81.04	0.90	2.39
C1 S6 x5	72	1056.77	8.59	106.85	0.014	261.99	1.23	0.02	0.0012	#VALUE!		64.23
C1 S7 x5	82	167.72	10.64	114.60	0.008	51.70	1.04	0.01	0.0004	#VALUE!	0.75	65.99
C1 S8 x5	92	165.39	11.27	123.12	0.009	38.59	1.10	0.01	0.0022	#VALUE!	0.61	63.85
C1 S9 x5	102	180.33	13.05	151.59	0.010	33.30	1.26	0.02	0.0005	#VALUE!	0.62	71.04
C1 S10 x5	112	87.50	10.84	131.09	0.013	27.79	1.19	0.02	0.0006	#VALUE!	0.57	56.27
C1 S11 x5	122	130.07	10.75	145.31	0.009	24.55	1.25	0.01	0.0005	250.50	0.51	53.70
C1 S12 x5	132	96.06	11.14	162.90	0.050	19.05	1.25		0.0068	200.95	2.64	51.16
C1 S13 x5	142	115.23	8.68	135.38	0.012	19.06	1.18	0.03	0.0009	187.08	0.67	41.34
C1 S14 x5	152	94.07	10.58	143.56	0.013	19.13	1.27	0.02	0.0009	186.66	0.56	48.96
C1 S15 x5	162	77.85	9.42	143.73	0.004	15.99	1.30	0.01	0.0005	149.80	0.45	41.48
C1 S16 x5	172	44.82	9.50	137.79	0.006	15.02	1.28	0.01	0.0006	141.84	0.44	41.15
C1 S17 x5	182	77.33	11.14	164.23	0.006	15.79	1.33	0.02	0.0005	147.43	0.63	48.15
C1 S18 x5	192	105.61	10.44	179.28	0.012	15.94	1.35	0.02	0.0010	148.03	0.72	44.93
C1 S19 x5	202	100.88	6.96	132.85	0.011	13.07	1.26	0.02	0.0007	124.02	0.41	29.95
C1 S20 x5	212	151.35	9.21	156.95	0.033	16.22	1.39	0.09	0.0016	174.29	1.31	38.08
C1 S22 x5	232	56.02	8.32	112.22	0.009	12.27	1.31	0.02	0.0006	118.98	0.73	34.48
C1 S23 x5	242	91.45	11.33	165.74	0.048	14.06	1.52	0.13	0.0028	125.13	1.80	46.02
C1 S24 x5	252	68.73	9.23	156.47	0.006	12.76	1.37	0.01	0.0006	99.12	0.42	36.54
C1 S25 x5	262	63.75	6.34	105.50	0.004	9.58	1.27	0.01	0.0006	93.63	0.40	24.94
C1 S26 x5	272	79.19	7.91	137.98	0.012	9.61	1.41	0.04	0.0011	93.37	0.85	31.82
C1 S27 x5	282	0.53	2.87	15.18	0.013	9.05	1.25	0.02	0.0008	99.83	0.82	12.99

Table 11. ICP-OES geochemistry results (bottom column)

	Day	Al	Ba	Ca	Fe	K	Li	Mg	Mn	Na	S	Sr
C3 S1 x500	16	568.01	1.16	585.84	1.15	85.22	7.77	3.14	0.07	1288.77	30.51	4.14
C3 S2 x500	30	45.41	0.80	288.05	0.81	25.50	4.56	0.58	0.04	152.41	14.69	3.14
C3 S3 x500	42	33.97	0.49	285.01	0.72	23.17	5.19	0.54	0.05	135.65	15.01	2.21
C3 S4 x500	52	72.28	0.25	303.38	0.54	19.09	5.87	0.55	0.04	93.61	12.07	1.53
C1 S5 x250	62		18.65	186.02	0.60	52.15	3.22	0.66	0.06		23.16	79.47
C3 S6 x500	72		0.02		0.08	1.49	0.79	0.06	0.00		1.58	0.13
C3 S7 x500	82	30.15	0.15	327.18	0.52	13.69	7.75	0.45	0.03	72.13	15.39	0.97
C3 S8 x500	92	20.64	0.14	333.72	0.53	11.20	7.76	0.39	0.04	58.03	13.03	0.96
C3 S9 x500	102	62.97	0.28	344.02	1.49	7.89	6.10	2.48	0.06	67.26	18.08	0.83
C3 S10 x500	112	28.25	0.75	298.84	0.52	10.54	7.65	0.77	0.05	60.03	16.34	0.74
C3 S11 x500	122	30.47	0.18	255.25	0.53	10.13	8.31	0.48	0.05	58.56	14.09	0.47
C3 S12 x500	132	46.30	0.17	270.43	0.47	10.05	8.19	0.51	0.05	57.22	17.57	0.57
C3 S13 x500	142	23.67	0.10	263.88	0.50	54.45	7.34	0.49	0.05	54.75	16.12	0.44
C3 S14 x500	152	46.91	0.16	261.51	0.40	54.03	7.00	0.52	0.06	54.20	16.09	0.49
C3 S15 x500	162	14.70	0.24	216.68	0.57	56.73	6.43	0.54	0.07	55.62	17.80	0.54
C2 S8 x1000	172		0.16		0.53	410.04	1.81	0.48	0.05		89.24	0.36
C3 S17 x500	182	35.84	0.12	275.58	0.64	53.69	7.13	0.73	0.05	52.68	17.97	0.28
C3 S18 x500	192	24.25	0.19	227.33	0.60	55.67	6.62	0.67	0.03	61.32	18.51	0.41
C3 S19 x500	202	7.41	0.18	215.79	0.65	54.45	5.74	0.57	0.06	56.20	17.65	0.30
C3 S20 x500	212	50.33	0.24	265.19	0.69	56.23	6.97	0.70	0.05	57.02	16.75	0.42
C3 S21 x500	222	33.79	0.18	223.78	0.57	55.71	7.19	0.57	0.05	63.98	14.78	0.23
C3 S22 x500	232	16.65	0.20	181.91	0.51	54.42	7.61	0.42	0.04	55.72	15.55	0.38
C3 S23 x500	242	58.15	0.67	292.33	0.56	55.45	7.71	0.77	0.04	61.24	16.45	1.59
C3 S24 x500	252	39.50	0.17	194.93	0.42	51.17	6.33	0.50	0.05	48.96	16.74	0.57
C3 S25 x500	262	26.97	0.13	140.71	0.40	51.03	5.19	0.70	0.03	50.18	18.97	0.20
C3 S26 x500	272	42.73	0.09	213.04	0.43	52.12	7.26	0.50	0.04	51.75	17.74	0.29
C3 S27 x750	282	5.60	0.17		0.51	70.95	7.58	0.59	0.05	70.94	23.18	0.21
C3 S1 x15	16	600.92	1.00	552.52	0.39	119.85	6.61		0.02	1231.83	14.42	4.97
C3 S2 x15	30	43.49	0.46	239.42	0.02	32.00	2.76	0.20	0.00	124.05	1.75	3.47
C3 S3 x15	42	33.63	0.25	251.28	0.02	31.48	3.72	0.07	0.00	115.66	1.13	2.72
C3 S4 x15	52	75.08	0.08	261.40	0.02	24.40	4.21	0.10	0.00	66.85	0.87	1.76
C3 S5 x15	62	144.41		176.71	0.03	78.07	0.98	0.03	0.00		1.14	
C3 S6 x15	72	53.02	0.05	309.09	0.02	19.74	6.62	0.04	0.00	50.59	0.78	1.45
C3 S7 x15	82	27.34	0.04	261.25	0.01	15.61	6.07	0.04	0.00	36.99	0.80	1.17
C3 S8 x15	92	19.11	0.04	274.71	0.02	13.50	6.28	0.04	0.00	32.02	0.74	1.05
C3 S9 x15	102	67.08	0.06	301.56	0.16	10.48	4.80		0.01	40.41	4.42	0.91
C3 S10 x15	112	25.45	0.04	237.29	0.02	12.46	5.89	0.08	0.00	29.35	1.09	0.79
C3 S11 x15	122	27.92	0.03	204.77	0.01	12.11	6.29	0.06	0.00	26.98	0.84	0.67
C3 S12 x15	132	44.43	0.02	219.41	0.01	11.95	6.44	0.08	0.00	27.28	0.98	0.67
C3 S13 x15	142	21.68	0.02	217.84	0.02	12.09	6.36	0.05	0.00	24.28	0.77	0.61
C3 S14 x15	152	45.46	0.02	218.19	0.02	12.02	5.91	0.14	0.00	23.29	1.45	0.58
C3 S15 x15	162	11.85	0.02	182.24	0.02	10.65	5.11	0.09	0.00	21.03	1.49	0.46
C3 S16 x15	172	4905.93	0.03	0.71	0.01		0.45	0.01	0.01			0.27
C3 S17 x15	182	34.68	0.02	227.13	0.02	11.73	6.17	0.12	0.00	21.59	1.50	0.50
C3 S18 x15	192	18.91	0.02	169.82	0.02	10.70	4.88	0.17	0.00	24.14	2.41	0.38
C3 S19 x15	202	4.59	0.02	169.66	0.02	10.12	4.08	0.17	0.00	22.36	2.94	0.33
C3 S20 x15	212	46.71	0.02	210.75	0.02	11.33	5.61	0.30	0.00	22.57	2.42	0.46
C3 S21 x15	222	30.45	0.05	177.94	0.02	12.39	5.82	0.16	0.00	31.41	2.13	0.42
C3 S22 x15	232	12.87	0.01	150.42	0.02	12.02	6.32	0.08	0.00	22.50	1.94	0.39
C3 S23 x15	242	58.46		236.23	0.04	13.17	6.61	0.35	0.00	32.54	3.16	
C3 S24 x15	252	38.47	0.02	165.99	0.03	11.73	5.32	0.21	0.00	22.33	2.88	0.34
C3 S25 x15	262	24.75	0.01	119.25	0.02	9.30	3.79	0.38	0.00	21.34	3.96	0.25
C3 S26 x15	272	40.60	0.02	175.55	0.02	10.83	6.12	0.24	0.00	23.40	2.99	0.38

Blank values were outlier not used for plots, red values were over calibration curve and green values were the samples used for plotting.

Table 12. Results from ICP-OES runs of 3 certified reference materials and their precision (RSD) and accuracy (as defined in Appendix D)

Certified reference material 1*	Al	Ba	Ca	Fe	K	Li	Mg	Mn	Na	S	Sr
Measured - Replicate 1	0.047	0.029	0.143	0.016	0.081	0.029	0.084	0.046	0.460	0.048	0.050
Measured - Replicate 2	0.049	0.029	0.144	0.017	0.082	0.029	0.085	0.046	0.466	0.041	0.050
Measured - Replicate 3	0.047	0.029	0.145	0.016	0.082	0.029	0.085	0.046	0.467	0.046	0.050
Measured - Replicate 4	0.048	0.029	0.145	0.017	0.167	0.026	0.085	0.046	0.466	0.045	0.050
Measured - Replicate 5	0.048	0.029	0.144	0.017	0.167	0.026	0.085	0.046	0.467	0.043	0.050
Measured - Replicate 6	0.048	0.029	0.146	0.017	0.167	0.026	0.085	0.046	0.467	0.039	0.050
Expected Value (500x)	0.038	0.020	0.153	0.010	0.090	0.019	0.075	0.040	0.413		0.051
Accepted Concentrations	0.0323 - 0.0485	0.0175 – 0.0232	0.111 – 0.304	0.0060 – 0.0157	0.024 – 0.188	0.0137 – 0.0232	0.0614 – 0.111	0.0359 – 0.04334	0.264 – 0.534		0.0241 – 0.0292
Mean	0.048	0.029	0.144	0.017	0.125	0.028	0.085	0.046	0.466	0.044	0.050
Std Dev	0.0005	0.0001	0.0009	0.0005	0.0467	0.0014	0.0003	0.0002	0.0029	0.0032	0.0003
Precision (RSD)	1.0%	0.3%	0.6%	3.2%	37.5%	4.9%	0.4%	0.4%	0.6%	7.3%	0.6%
Accuracy	24.4%	44.2%	-7.0%	66.6%	36.3%	43.2%	11.2%	12.8%	11.0%		-3.4%
Certified reference material 2**											
Measured - Replicate 1	0.243	3.956	6.947	1.168	3.711	0.146	7.207	0.336	16.223	0.166	0.976
Measured - Replicate 2	0.245	3.971	6.962	1.151	3.718	0.146	7.199	0.336	16.202	0.175	0.981
Measured - Replicate 3	0.243	3.964	6.892	1.160	3.698	0.133	7.166	0.336	16.247	0.160	0.972
Measured - Replicate 4	0.242	3.939	6.882	1.157	3.669	0.133	7.145	0.336	16.200	0.175	0.962
Measured - Replicate 5	0.242	3.938	6.888	1.157	3.678	0.133	7.158	0.336	16.221	0.174	0.967
Measured - Replicate 6	0.233	3.350	7.690	1.290	3.190	0.104	6.920	0.345	19.100		0.916
Expected Value (50x)	0.233	3.348	7.686	1.289	3.188	0.104	6.917	0.345	19.091		0.916
Accepted Concentrations	0.199 – 0.268	1.55 – 1.94	7.00 – 8.38	1.17- 1.41	2.76 – 3.63	0.0840 – 0.124	6.31 – 7.52	0.318 – 0.373	17.4 – 20.8		0.789 – 1.043
Mean	0.243	3.953	6.914	1.159	3.695	0.138	7.175	0.336	16.219	0.170	0.971
Std Dev	0.0012	0.0150	0.0373	0.0064	0.0212	0.0071	0.0270	0.0004	0.0191	0.0065	0.0076
Precision (RSD)	0.5%	0.4%	0.5%	0.6%	0.6%	5.2%	0.4%	0.1%	0.1%	3.8%	0.8%
Accuracy	4.4%	18.1%	-10.0%	-10.1%	15.9%	32.9%	3.7%	-2.6%	-15.0%		6.1%
Certified reference material 3***											
Measured - Replicate 1	0.013	0.0011	3.690	0.007	6.079	0.006	13.804	0.001	124.174	10.629	0.170
Measured - Replicate 2	0.014	0.0011	3.647	0.007	6.056	0.006	13.695	0.001	123.919	10.619	0.169
Measured - Replicate 3	0.014	0.0011	3.678	0.007	5.991	0.005	13.721	0.001		10.692	0.168
Measured - Replicate 4	0.014	0.0011	3.672	0.007	5.992	0.005	13.653	0.001		10.747	0.166
Measured - Replicate 5	0.012	0.0011	3.677	0.007	5.959	0.005	13.649	0.001		10.644	0.166
Expected Value	0.5	0.1	400.0	0.020	380.0	0.1	1250.0	0.010	10500.0	900.0	12.0
Mean	0.0138	0.0011	3.6718	0.0068	6.0297	0.0053	13.7182	0.0007	124.0465	10.6718	0.1682
Std Dev	0.000502393	1.28938E-05	0.01787644	0.000154515	0.04484295	0.0002978	0.06352135	1.22848E-05	0.18015313	0.059832385	0.00145312
RSD	3.6%	1.2%	0.5%	2.3%	0.7%	5.6%	0.5%	1.8%	0.1%	0.6%	0.9%
Accuracy	179.0%	124.7%	-7.5%	3332.6%	60.0%	434.7%	10.6%	593.8%	19.1%	19.5%	41.3%

*Certified reference material 1 is a low concentration ground water certified reference material (ES-L-2, EnviroMAT ground water low, certified reference material)
**Certified reference material 2 is a high concentration ground water certified reference material (ES-H-3, EnviroMAT certified reference material)
***Certified reference material 3 is a seawater certified reference material (CRM-SW, sea water, certified reference material)

Table 13. IC geochemistry results (top column)

Top Column	Day	F	Cl	NO3
C2 S3	16	29.8		
C2 S4	30	13.8	225.9	9.0
C2 S5	42	174.4	218.6	17.0
C2 S6	52	398.8	208.3	4.1
C2 S7	62	77.1	72.0	1.7
C2 S8	72	25.4	37.9	2.6
C2 S9	82	43.7	49.0	2.5
C2 S10	92	704.2	6.8	21.2
C2 S11	102	12.9	28.4	3.4
C2 S12	112	11.3	21.5	2.5
C2 S13	122	4.1	5.1	25.0
C2 S14	132	6.0	22.1	54.9
C2 S15	142	8.7	7.3	42.4
C2 S16	152	11.6	27.0	17.7
C2 S17	162	9.0	25.4	21.7
C2 S18	172	8.2	22.7	23.8
C2 S19	182	4.4	20.0	24.8
C2 S20	192	5.6	24.0	27.1
C2 S21	202	7.4	23.8	24.5
C2 S22	212	5.9	24.5	27.1
C2 S23	222	4.5	22.9	28.2
C2 S24	232	4.8	22.5	28.5
C2 S25	242	4.7	22.3	30.3

Table 14. IC geochemistry results (middle column)

Middle Column	Day	F	Cl	NO3
C1 S1	16	4.4	24.6	29.6
C1 S2	30	2.0	23.2	28.2
C1 S3	42	4.7	17.7	
C1 S4	52	5.6	17.5	27.3
C1 S5	62	9.0	14.9	33.7
C1 S6	72	8.3	11.3	38.1
C1 S7	82	8.2	8.9	32.6
C1 S8	92	6.4	7.1	28.5
C1 S9	102	5.6	7.2	29.5
C1 S10	112	5.3	7.4	27.9
C1 S11	122	4.1	5.1	25.0
C1 S12	132	6.0	22.1	54.9
C1 S13	142	8.7	7.3	42.4
C1 S14	152	9.4	7.8	41.4
C1 S15	162	7.2	6.5	36.9
C1 S16	172	7.8	6.1	37.6
C1 S17	182	4.3	6.6	36.8
C1 S18	192	3.7	6.2	34.8
C1 S19	202	5.0	7.5	43.3
C1 S20	212	5.8	7.8	47.6
C1 S21	222	5.4	6.6	43.0
C1 S22	232	5.5	6.1	43.1
C1 S23	242	5.6	6.1	45.1
C1 S24	252	6.8	6.1	44.4
C1 S25	262	7.4	7.6	47.9
C1 S26	272	6.5	7.2	42.9
C1 S27	282	6.4	7.1	43.9

Table 15. IC geochemistry results (bottom column)

Bottom Column	Day	F	Cl	NO3
C3 S1	16	1.0	8.2	43.6
C3 S2	30	0.4	8.0	31.9
C3 S3	42	0.7	5.7	19.6
C3 S4	52	0.7	4.0	16.2
C3 S5	62	0.6	4.5	14.4
C3 S6	72	0.7	4.1	20.8
C3 S7	82	0.7	3.4	17.0
C3 S8	92	0.8	3.0	19.8
C3 S9	102	0.5	18.0	28.6
C3 S10	112	0.7	7.1	21.6
C3 S11	122	0.7	5.1	28.3
C3 S12	132	0.3	5.3	33.3
C3 S13	142	0.9	4.5	23.2
C3 S14	152	0.5	6.0	32.4
C3 S15	162	0.7	5.4	31.1
C3 S16	172	1.2	6.8	21.2
C3 S17	182	0.8	4.7	28.7
C3 S18	192		6.8	36.8
C3 S19	202		6.4	39.7
C3 S20	212	1.0	6.1	39.0
C3 S21	222	1.0	6.2	36.8
C3 S22	232	1.1	5.8	36.9
C3 S23	242	1.1	5.9	38.1
C3 S24	252	1.3	5.7	38.7
C3 S25	262		8.6	44.5
C3 S26	272	0.9	6.1	40.4
C3 S27	282	1.2	6.3	39.7

Table 16. ICP-MS results for top column

Sample Code	Day	Li	Na	Mg	Al	Cl	K	Ca	Ti	Mn	Fe	Br	Sr	Ba	Th	U	Ce
C2 S3	42	76.74046142	19745.11086	1.983281838	4037.21271	1179.077487	382.9176051	38.68308883	0.056179183	0.039012207	3.492843578	1773.476835	0.031592893	0.357488825	0.00023835	7.9517E-05	0.18682738
C2 S4	56	435.1553557	12204.87381	1.336430756	3527.500442	417.8276316	165.5852271	35.83761225	0.042375358	0.054710887	2.30458213	1014.326624	0.490946369	0.247647819	0.007645997	0.005814372	0.54756682
C2 S5	70	642.9444883	6503.222179	1.239027026	2054.630773	798.2605338	97.81515449	35.60829375	0.031720168	0.003855573	1.729132427	553.164629	1.221152523	0.879479114	0.000206152	4.68576E-05	0.20233003
C2 S6	82	1166.014202	2056.225291	1.215485737	641.7105514	1060.069861	36.66544047	36.80118752	0.033577556	0.004122404	1.444782139	215.6674338	4.257010362	0.860886585	0.000263621	7.02347E-05	0.45750438
C2 S7	94	805.6524891	3648.302661	1.391007027	1155.371741	262.9296674	59.74812739	34.0864073	0.026416473	0.008747037	1.291224659	331.2125846	2.063562343	0.402431005	0.000134051	0.000106549	0.17882829
C2 S8	108	274.5086231	23423.44199	0.893677247	5855.515363	910.9371456	277.8589202	29.97583036	0.069228578	0.013288143	-0.009955928	2316.573528	0.194033505	0.079501492	0.000193033	0.010990262	0.58050453
C2 S9	122	1590.460354	1460.187522	1.296992935	418.4576429	437.8931342	27.58213047	40.15173587	0.032155754	0.136277654	8.187977928	172.3856965	8.058708781	1.195073325	0.00017167	4.97848E-05	0.32403387
C2 S10	134	2441.89324	1109.088924	1.942031188	301.0725083	654.4289249	24.50130444	43.91052316	0.054650591	0.010444329	0.695402119	145.1099153	5.151495716	1.559580167	0.000194439	3.3447E-05	0.18263910
C2 S11	146	2095.944046	859.367807	1.131141801	144.003006	304.5285682	16.35899634	34.84509745	0.029641088	0.023421632	1.753898715	118.4175175	2.575274818	0.441076223	0.000157271	2.67203E-05	0.10183893
C2 S12	158	1041.263697	681.679849	1.491774062	7.973143277	527.6616479	14.4011407	41.14018447	0.024848057	0.006380073	0.669211354	100.4475483	4.11580463	1.8200445	0.000185944	2.49366E-05	0.41289591
C2 S13	168	2922.489746	654.7331806	1.609852172	106.5037815	508.9711413	14.075257	34.04462678	0.029824409	0.012891443	1.931991472	113.6443325	1.081885961	0.252749835	0.000154527	3.02832E-05	0.17156033
C2 S14	180	5138.702909	610.8037999	0.169110409	137.7125747	665.9136762	11.1104145	5.633611873	0.011262768	0.002073039	-0.207544474	125.3150746	2.272372492	0.381006779	0.000151058	2.31783E-05	0.20683975
C2 S15	192	11197.07658	477.0871996	0.109219595	103.1597036	602.2888472	8.346232861	105.0449199	0.018623756	0.046063773	7.685082678	107.2986844	121.5423464	31.13223977	9.58465E-05	6.18437E-05	1.01481754
C2 S16	204	7146.715809	392.4711877	0.150655451	87.25896502	439.6912519	7.92389629	104.7301809	0.032975576	-0.004144438	-0.342118371	99.75555742	109.4418534	30.15699265	0.000108282	4.85494E-05	0.80126680
C2 S18	216	7504.122746	354.2365584	0.98317081	95.32351108	6.348708937	13.19462107	88.73478713	0.030014549	0.001048837	3.161902439	94.23198858	100.0020507	25.22541519	0.00012762	4.15787E-05	0.43311159
C2 S19	228	8418.208556	352.4790296	0.275029466	91.73483626	5.587543537	8.726669562	68.89633919	-0.003754955	-0.016356018	3.482572397	104.1293074	79.65895715	21.73869584	0.00011258	3.41703E-05	0.42858392
C2 S20	238	8915.736279	290.2223637	0.913720754	79.98847772	306.8219899	6.877016415	39.14142027	0.006832408	0.022555319	2.442979155	79.0686508	61.71749466	18.65763825	9.95164E-05	1.89712E-05	0.37846730
C2 S21	250	8550.118904	228.610578	0.385204664	69.3461628	290.0930749	4.21915309	35.54060941	0.011903766	0.040568324	3.184134358	78.18293747	55.83584331	13.12963191	9.53205E-05	4.16428E-05	0.30302157
C2 S23	262	8918.649238	239.0418864	0.26929693	47.83126292	-14.18792233	4.701683025	6.074484843	0.01289573	0.000826641	1.04618329	94.9121393	7.929500361	1.042038398	7.34696E-05	9.15242E-06	0.27318309
C2 S24	272	932.4017585	116.9406701	0.286543868	23.2001258	59.0545122	7.689166165	147.2172593	0.005343143	-0.013608519	2.006974477	257.4811571	35.51946799	7.736378912	7.52344E-05	1.21355E-05	0.25920858
C2 S25	284	11053.6084	219.7550114	0.634956494	75.5572674	258.4078359	8.346557804	18.73326256	0.006737107	0.019808796	1.097380051	97.69687779	33.59938389	4.694623494	0.000109906	3.0731E-05	0.48856332

Red values are over calibration curve

Table 17. ICP-MS results for middle column

Sample Code	Day	Li	Na	Mg	Al	Cl	K	Ca	Ti	Mn	Fe	Br	Sr	Ba	Th	U	Ce
C1 S1	16	934.7879	2196.454	1.560416	1.996324	370.151	129.8061	255.2343	0.051634	0.018416	1.430929	8193.727	130.8053	22.72174	0.000224	7.69E-05	0.413171
C1 S2	30	644.7564	2100.389	1.767126	9.525617	1005.602	126.4771	136.3988	0.046267	0.038555	5.42126	7151.519	81.90474	13.80137	0.000327	7.55E-05	0.32208
C1 S3	42	489.0912	1727.488	1.378468	2.159504	853.8765	99.90892	58.56364	0.038011	0.00329	2.56694	5376.582	40.84858	6.051656	0.000238	7.95E-05	0.186827
C1 S4	52	558.2569	1473.448	1.268446	10.16362	257.8708	84.81648	42.08098	0.025877	0.001991	1.905896	4119.482	14.9735	2.151654	0.007646	0.005814	0.547567
C1 S5	62	502.4314	1073.191	3.36632	4.156487	976.9961	65.06563	37.15496	0.033917	0.061565	9.379818	2739.147	4.839335	0.936944	0.000206	4.69E-05	0.20233
C1 S6	72	540.3574	847.6206	1.732586	49.80351	450.8061	56.66914	43.631	0.035065	0.024693	3.022949	1995.031	8.604146	3.664699	0.000264	7.02E-05	0.457504
C1 S7	82	420.08	657.2458	1.418044	1.846237	352.3888	40.00856	32.15415	0.026888	0.016005	1.500118	1395.8	1.557434	0.383157	0.000182	2.33E-05	0.153188
C1 S8	92	598.4635	495.0023	1.158813	1.203399	328.0442	31.13904	38.92628	0.026484	0.005448	0.664973	1069.262	4.51699	0.571489	0.000203	3.4E-05	0.213624
C1 S9	102	556.8317	444.7977	2.11768	32.52412	698.6518	26.96047	54.37178	0.028285	0.00913	1.809497	903.8478	15.3154	2.97562	7.65E-05	3.21E-05	0.03142
C1 S10	112	468.2406	279.7565	1.088859	0.926803	608.1884	19.04766	34.68492	0.032832	0.005707	0.432976	616.0185	3.200761	0.361165	0.000189	2.73E-05	0.121099
C1 S11	122	570.3759	303.4613	1.128304	0.950024	754.4579	18.05592	40.1806	0.01777	8.96E-05	0.19599	626.8893	13.51368	2.185578	0.000181	3.56E-05	0.129394
C1 S12	132	763.9341	293.7621	1.90994	1.669275	680.2739	20.36343	56.27275	0.032779	0.010405	1.688872	520.2761	11.10309	1.416049	0.000142	3.94E-05	0.29966
C1 S13	142	717.9946	218.3886	1.224361	12.65733	911.8049	14.54373	50.39173	0.026754	0.012535	0.990302	484.5079	21.36713	3.720715	0.000157	3.44E-05	0.138891
C1 S14	152	684.0236	211.2256	1.133587	0.937979	307.7273	13.74157	45.35192	0.022823	-0.002564	-0.219694	450.1949	13.07847	2.323001	0.000704	0.000411	0.192784
C1 S15	162	798.8302	191.3501	1.188974	0.998232	279.9491	12.84895	49.92073	0.026812	0.004689	0.219595	406.649	18.14738	3.57361	0.000149	3.6E-05	0.235197
C1 S16	172	774.7671	172.6268	0.833131	0.969415	232.3128	10.13378	39.0917	0.024475	0.016857	0.335828	374.2579	12.48427	2.385614	0.000134	1.78E-05	0.099078
C1 S17	182	743.8076	162.108	0.785954	1.014419	771.8013	12.13179	44.76851	0.02714	0.090289	15.25629	372.6763	19.45836	3.910885	0.000149	2.94E-05	0.098434
C1 S18	192	772.7352	148.5983	0.807015	1.117619	444.619	11.19011	40.99931	0.021496	0.009638	1.091527	348.0049	17.7414	3.379913	0.000125	3.11E-05	0.115765
C1 S19	202	892.8851	173.1974	1.230696	1.071323	261.1496	11.70963	43.47982	0.023608	0.017659	0.087349	358.7673	18.16755	3.248908	0.000131	1.94E-05	0.128055
C1 S20	212	850.6737	162.4144	1.238623	6.535785	208.1871	12.19375	56.77941	0.02311	0.015095	0.966789	359.1223	19.85194	9.94608	0.000238	6.82E-05	1.038712
C1 S21	222	4447.499	41.7884	1.082495	5.544718	252.4322	12.80012	47.28207	0.102256	0.029887	1.934975	124.031	0.30449	0.121118	0.00014	2.91E-05	0.400185
C1 S22	232	967.5236	164.2261	1.262151	1.266716	222.5851	9.695496	38.77291	0.016901	0.0148	0.859906	379.7529	16.38322	3.043469	8.7E-05	1.68E-05	0.157645
C1 S23	242	890.6134	136.5691	0.82253	16.86132	139.2904	9.150306	38.18113	0.015955	0.013313	0.882816	325.3565	16.33719	2.974924	0.000131	2.16E-05	0.096318
C1 S24	252	874.1177	113.0976	0.067428	17.75642	408.6977	5.146036	153.366	0.048018	-0.008968	0.546677	253.0826	34.88238	7.115492	9.49E-05	1.44E-05	0.341318
C1 S25	262	840.4566	108.1585	0.465694	19.76798	338.8039	6.180519	95.42339	0.064004	0.001151	0.878459	246.6275	24.10963	5.032547	7.73E-05	2.66E-05	0.396485
C1 S26	272	894.2324	103.8851	0.119196	20.72894	448.0604	5.794496	133.3059	0.032541	-0.003603	0.613417	278.0479	29.49195	6.263139	9.02E-05	3.61E-05	0.41793
C1 S27	282	1785.137	248.7331	0.326813	1.640601	-38.2457	11.84251	35.64965	-0.005388	-0.00563	2.63594	506.7983	25.78511	5.080561	4.67E-05	3.52E-05	0.580782

Red values are over calibration curve

Table 18. ICP-MS results for bottom column

Sample Code	Day	Li	Na	Mg	Al	Cl	K	Ca	Ti	Mn	Fe	Br	Sr	Ba	Th	U	Ce
C3 S1	16	2727.536	162.5888	1.596151	2.170509	788.1888	44.79135	197.0104	0.042094	0.020922	4.496278	1197.279	2.371393	1.222416	0.000223	4.37E-05	0.478914
C3 S2	30	2353.117	181.2111	1.831065	3.916756	506.6425	41.98455	100.5849	0.045552	0.008927	4.20496	834.485	3.079221	0.840787	0.000258	4.25E-05	0.977133
C3 S3	42	2995.883	158.7767	1.77362	6.475524	1041.681	37.22732	77.79799	0.052673	0.069587	5.357161	633.4543	2.072459	2.03638	0.001027	0.00076	0.160791
C3 S4	52	3065.733	89.11505	1.450384	1.325184	960.7522	27.44707	67.68427	0.036414	0.008506	4.446126	373.2031	1.186406	1.918918	0.000877	0.000526	0.396899
C1 S5	62	7066.473	87.94673	1.255578	1.706789	239.5868	30.18263	105.2546	0.029314	0.002002	3.166871	576.6989	1.350659	0.085345	0.000235	6.23E-05	0.550233
C3 S6	72	4763.268	77.17248	1.500384	1.041457	688.8774	21.49046	70.81818	0.024624	0.004777	2.632324	353.5473	1.065797	0.076286	0.000172	3.12E-05	0.28319
C3 S7	82	4268.933	58.50013	1.189911	7.028272	768.1193	16.06715	82.87181	0.025053	0.001349	2.217568	281.3494	0.905657	0.289927	0.000162	1.44E-05	0.146541
C3 S8	92	5147.398	58.57293	1.196966	0.763846	966.1272	15.56044	82.20235	0.04215	0.00878	0.918239	306.3403	0.893653	0.049139	0.000144	5.1E-05	0.129405
C3 S9	102	3302.073	61.1023	2.460982	8.414117	705.0887	10.17476	68.77786	0.033303	0.029456	1.983465	155.109	0.497931	0.086957	0.000103	3.45E-05	0.194524
C3 S10	112	4654.193	48.15919	1.169699	0.841318	213.3827	13.2456	62.92885	0.028001	0.002765	0.579628	199.8134	0.643653	0.093452	0.000133	2.91E-05	0.105828
C3 S11	122	4547.828	46.63301	1.291115	1.39046	183.1211	12.11478	68.72722	0.025203	0.010302	0.766895	190.125	0.518761	0.213492	0.00012	4.21E-05	0.155958
C3 S12	132	4792.293	52.94864	1.472537	3.883297	906.3604	13.33518	65.68547	0.024924	0.008268	0.762613	182.3816	0.501796	0.150521	0.000128	2E-05	0.120625
C3 S13	142	4753.457	42.12049	1.103465	0.573068	532.5812	11.36033	66.39837	0.008947	-0.00243	0.316618	180.1434	0.405805	0.031772	0.000118	2.94E-05	0.1334
C3 S14	152	4375.69	41.53306	1.599046	2.524774	494.0845	11.75739	70.6928	0.073237	0.031325	0.711758	155.8668	0.433172	1.649122	0.000158	3.72E-05	0.298952
C3 S15	162	4090.681	39.70318	1.036781	4.840373	208.8846	10.78328	51.34264	0.02963	0.00174	0.180933	138.4656	0.344514	0.70166	0.000134	3.77E-05	0.363036
C2 S8	172	4274.74	44.27302	1.397418	4.768843	834.5307	11.15721	69.23722	0.03208	0.019193	3.262503	149.9761	0.315864	0.073401	0.000125	1.7E-05	0.164938
C3 S17	182	4949.064	33.5333	1.324485	1.11704	184.6037	12.30485	49.94154	0.019013	0.007164	0.910247	155.3818	0.315784	0.334383	0.000204	3.78E-05	0.530167
C3 S18	192	3703.874	36.12997	0.868576	0.934657	637.7123	10.92671	50.77056	0.046971	-0.002749	0.225415	120.7561	0.265152	0.041009	0.000106	2.42E-05	0.311325
C3 S19	202	3046.202	34.99634	0.830669	1.928603	548.0968	9.27467	46.24092	0.041709	0.007985	0.356849	99.60269	0.240031	0.020229	0.000122	2.8E-05	0.261174
C3 S20	212	3520.019	34.16748	1.060805	5.15541	536.6067	10.53165	44.34077	0.195408	0.007225	0.76846	109.6504	0.249745	0.029107	0.000117	3.15E-05	0.506474
C3 S21	222	4861.232	38.10213	1.033934	0.804758	507.7312	10.17714	44.73906	0.073599	0.139856	7.761002	131.271	0.284887	0.029802	0.000148	4.27E-05	0.351349
C3 S22	232	4636.73	36.89819	0.972543	6.90989	645.4158	10.20438	47.03659	0.079629	0.006335	0.308455	124.5279	0.226384	0.053838	0.000139	3.74E-05	0.313884
C3 S23	242	4414.429	36.32483	0.864538	0.558472	433.8264	10.10521	52.89127	0.073135	-0.003761	0.044263	129.0233	0.274933	0.030682	0.000108	3.58E-05	0.327838
C3 S24	252	4229.744	24.03144	0.169715	10.87336	341.9218	7.203697	144.3043	0.034617	-0.005801	0.744573	104.473	0.324489	0.04719	8.63E-05	3.81E-05	0.428022
C3 S25	262	3024.206	22.11291	0.245596	7.864885	363.5108	6.994432	100.8386	0.038961	-0.005794	-0.361035	86.39674	0.238671	0.011705	5.18E-05	1.93E-05	0.366216
C3 S26	272	4602.843	22.81361	0.263409	9.177742	365.5965	8.163172	130.0437	0.023451	-0.007435	0.71205	109.6322	0.33128	0.01108	5.78E-05	7.57E-06	0.208248
C3 S27	282	8454.139	56.98992	0.259235	2.678976	-10.28051	16.38504	28.56005	0.010126	-0.008426	1.243955	217.4625	0.411969	0.328443	8.26E-05	3.59E-05	0.535081

Red values are over calibration curve

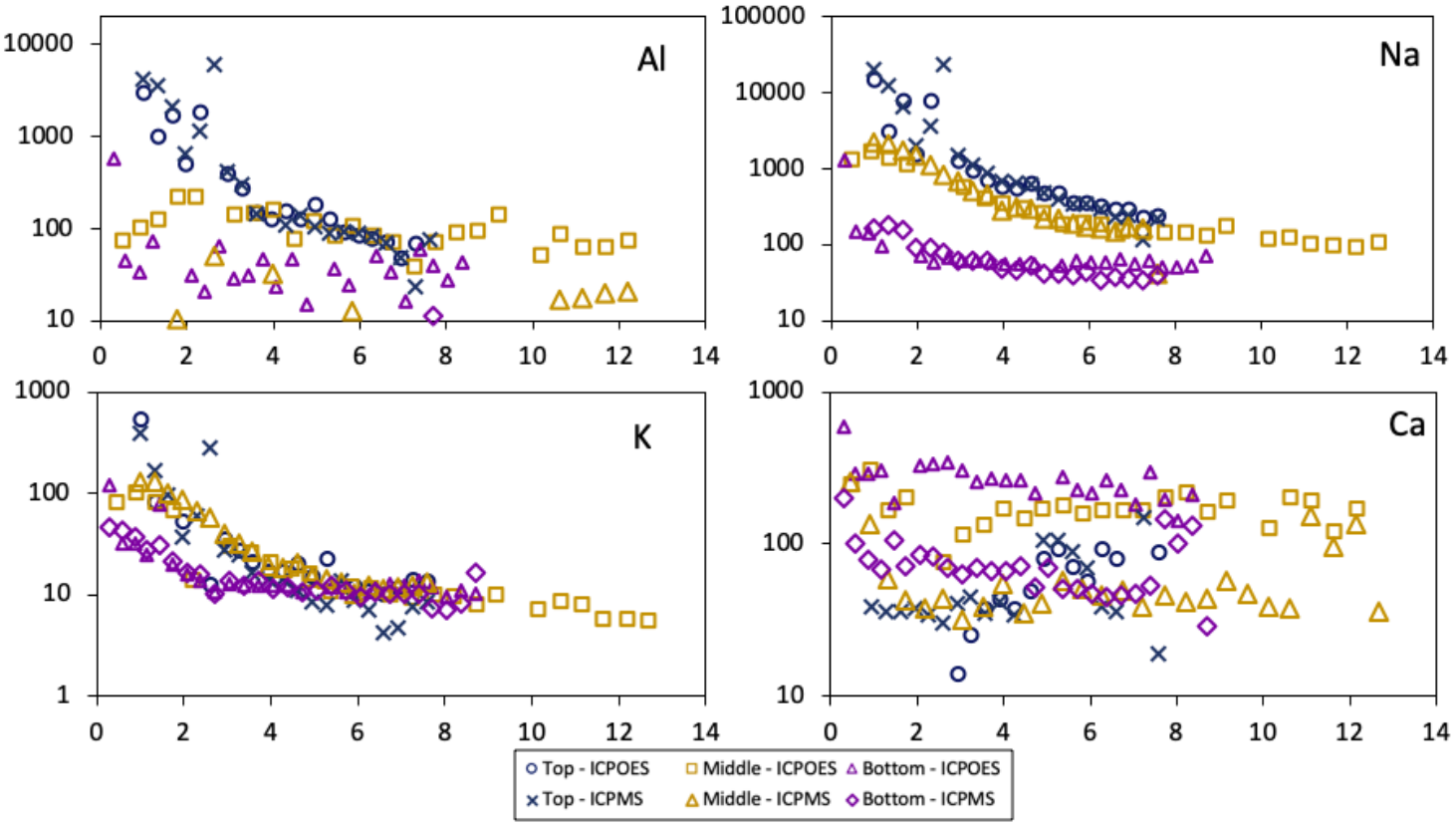

Figure 22. Comparison of ICP-MS and ICP-OES results for select element

Appendix D: Data Quality Analysis

D.1 Accuracy

In order to assess accuracy of the methods discussed in Appendix A and B, samples of known concentrations were analyzed during each analysis. The RE was calculated for each analyte and according to the following equation (i) and the results are in Table 12 (Skoog et al. 1998).

$$\text{Relative error } (\%) = \frac{\text{Actual Concentration} - \text{Measured Concentration}}{\text{Actual Concentration}} \quad \text{x} \quad 100\% \quad \text{[i]}$$

D.2 Precision

In order to assess precision of the analysis discussed in Appendix A and B, measurements of standards were replicated. The precision was calculated as RSD and is calculated by the formula i and ii (Skoog et al. 1998) results are in Table 12.

$$\text{RSD} = \frac{\sigma}{\mu}\ x\ 100\% \quad \text{[i]}$$

Where,

$$\sigma = \text{standard deviation}$$

$$\mu = \text{mean}$$

$$\sigma = \sqrt{\frac{(n\sum x_i^2 - (\sum x_i)^2)}{n(n-1)}} \quad \text{[ii]}$$

Where,

$$\text{x} = \text{concentration of i}^{\text{th}}\text{sample}$$

$$\text{n} = \text{number of measurements}$$

D.3 References

Skoog D. A., Holler F. J., and Nieman T. A. 1998 *Principles of Instrumental Analysis.* Saunders College Publishing.

Appendix E: Microprobe Analysis

E.1 Results

EPMA analysis was used to determine if there were significant concentrations of U or Th in the secondary minerals. Results in Table 16 are from the top mineralogical sample and indicate low concentrations of U and Th thoughout the secondary material.

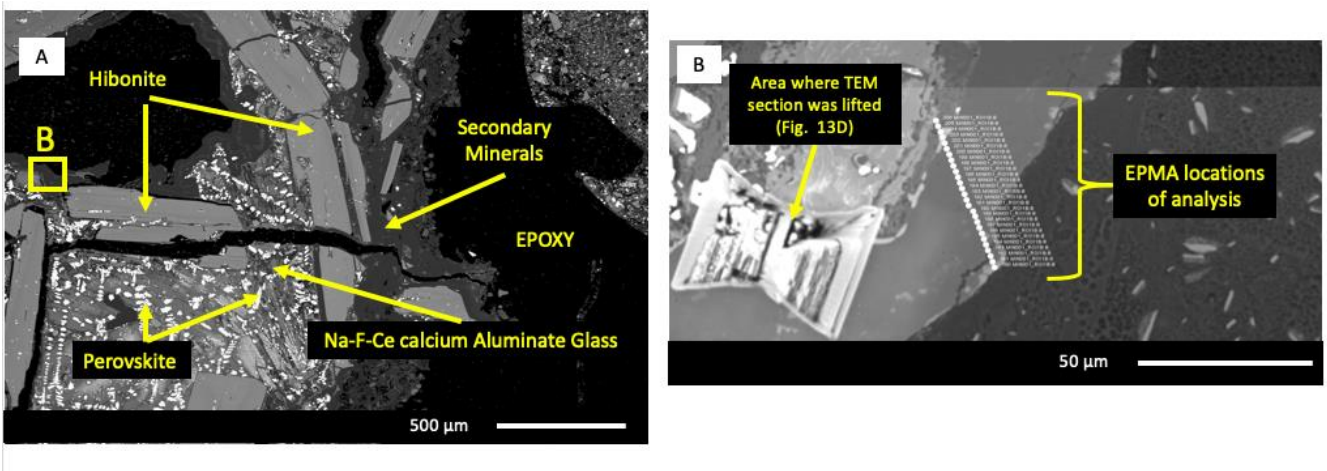

Figure 23. A) low magnification SEM BSE image B) EPMA location of analysis labelled B on image A

Table 16. Summary statistics microprobe analysis of secondary material in top sample. Results are shown in percent of total composition.

	UO_2 (%)	ThO_2 (%)
Average	0.00	0.00
StdDev	0.00	0.00
StdErr	0.00	0.00
Minimum	0.00	0.00
Maximum	0.01	0.02

Appendix F: X-Ray Diffraction Analysis

F.1 Methods

X-Ray Diffraction (XRD) was used to determine the primary mineralogy of the slag. A detailed description of the sampling methods used to obtain the slag for X-ray analysis is provided in Chapter 2. All analyses were collected on pulverized bulk sample. Diffraction patterns were collected using a Cu anode from 4.5˚ to 90.0˚ (2θ) using a step size of 0.02˚ and an integration time of 17 s.

F.2 Results

In general, the XRD results were similar between the top and middle samples and differed greatly from those collected at the bottom of the slag. The large compositional variations in the main phases is a result of distinct mineralogy between the top, middle, and bottom samples. According to the XRD patterns, the main phases within the slag are hibonite (0-59%), perovskite (0-35%), and gehlenite (0-31%), although ferri-gehlenite is more probable based on SEM and TEM work for this study (Fig. 19-21).

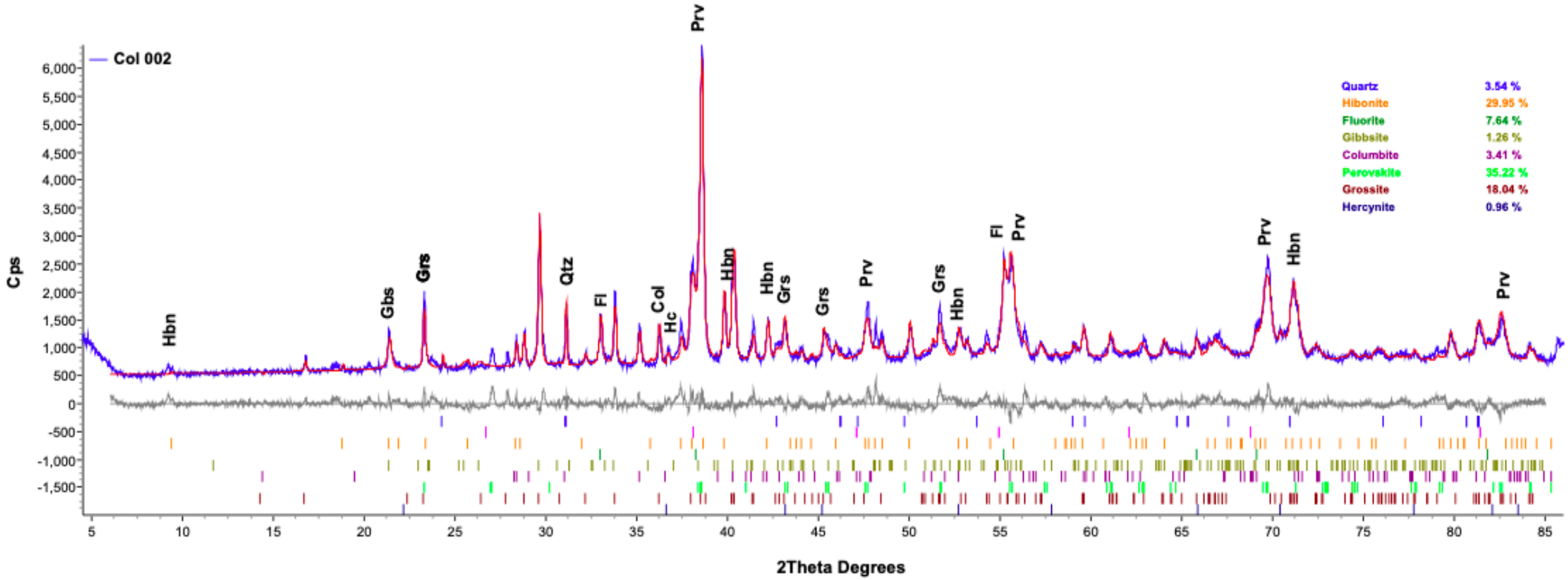

Figure 24. XRD from top column sample

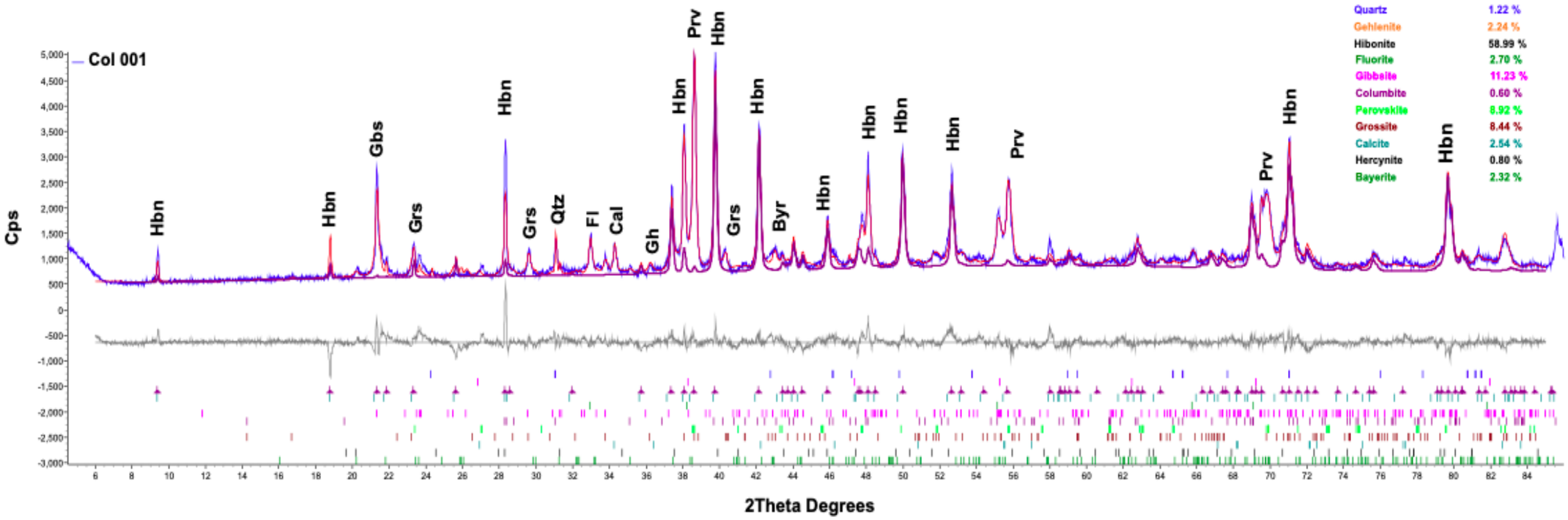

Figure 25. XRD spectra from middle column sample

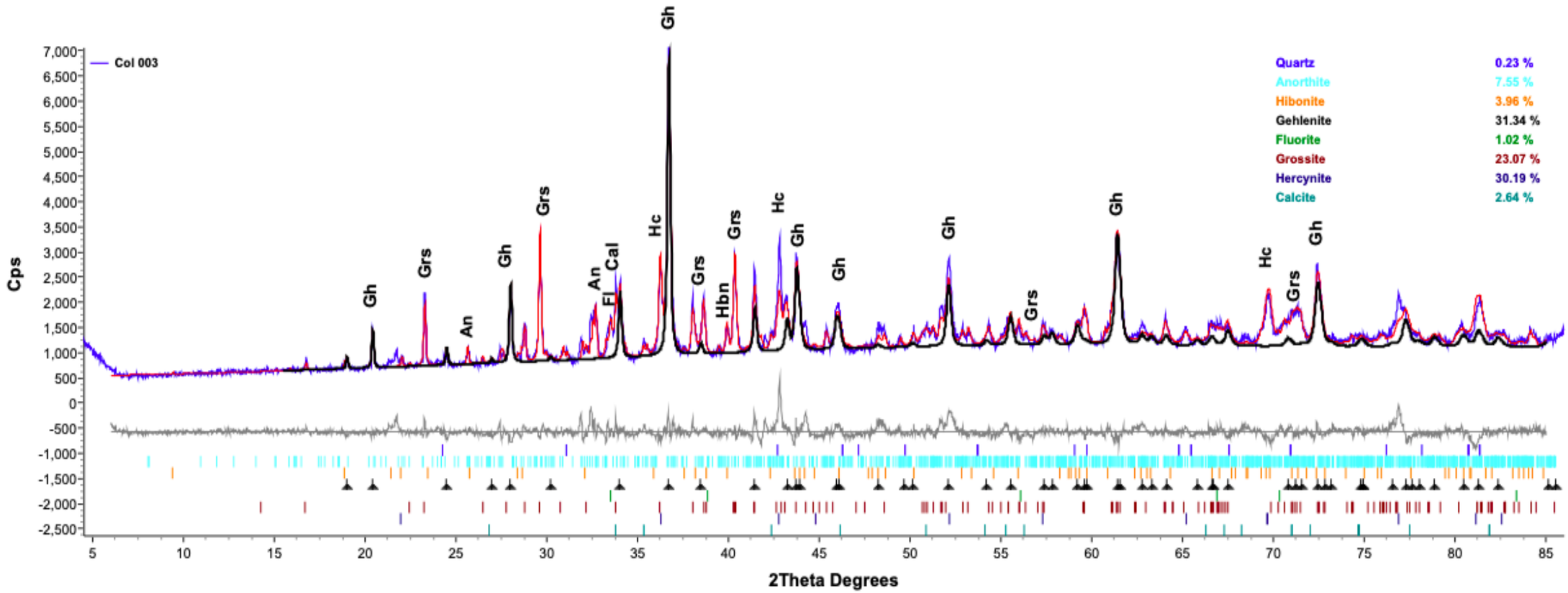

Figure 26. XRD spectra of bottom columns sample